Palaeogeography, Palaeoclimatology, Palaeoecology 512 (2018) 56–70

Contents lists available at ScienceDirect

Palaeogeography, Palaeoclimatology, Palaeoecology

journal homepage: www.elsevier.com/locate/palaeo

Mid-Pliocene global land monsoon from PlioMIP1 simulations

Xiangyu Li[a], Dabang Jiang[a,b,c,*], Zhiping Tian[a], Yibo Yang[b,d]

[a] Institute of Atmospheric Physics, Chinese Academy of Sciences, Beijing 100029, China
[b] CAS Center for Excellence in Tibetan Plateau Earth Sciences, Beijing 100101, China
[c] Collaborative Innovation Center on Forecast and Evaluation of Meteorological Disasters, Nanjing University of Information Science & Technology, Nanjing 210044, China
[d] Key Laboratory of Continental Collision and Plateau Uplift, Institute of Tibetan Plateau Research, Chinese Academy of Sciences, Beijing 100101, China

ARTICLE INFO

Keywords:
Mid-Piacenzian
Pliocene
Carbon cycle
Climate feedback
Major Northern Hemisphere glaciation
Reconstruction

ABSTRACT

The mid-Piacenzian (Pliocene) warm period (approximately 3.3–3.0 Ma) monsoon not only provides us with a useful insight into the future monsoon under a warming scenario with high atmospheric CO_2 concentration but is also hypothesized to play a key role in climate feedback through impact on the carbon cycle on a geological timescale. The monsoon evolution over time is one key to test this hypothesis. In this sense, we examine the mid-Piacenzian global land monsoon area (GLMA), precipitation (GLMP), and GLMP intensity (GLMPI) using all available model data from the Pliocene Model Intercomparison Project phase 1 (PlioMIP1). Relative to the pre-industrial period, both the GLMA and GLMP increase in the mid-Piacenzian and by an average of 7.3% and 5.8%, respectively. On a large scale, the increased GLMP comes mainly from northern Africa, Asia, and northern Australia. Quantitatively, it is the variation of GLMA, not of GLMPI, that makes a major contribution to the GLMP change. Further analysis reveals that anomalous inland water vapor transportation due to the reduced large-scale meridional thermal contrast in the mid-to-upper troposphere, together with the variation of vertical moisture advection and evaporation, explains most of the global land monsoon changes. A model–data comparison shows that the simulated monsoon precipitation variations are roughly consistent with the reconstructions in northern Africa, Asia, northern Australia, Central America, and eastern South America. Moreover, the intensified mid-Piacenzian Asian monsoon, which is supported by both simulations and reconstructions, or an overall intensified global land monsoon is hypothesized to contribute to the lowering of atmospheric CO_2 concentration and the subsequent onset of the sustained major Northern Hemisphere glaciation.

1. Introduction

Mostly located in tropical and subtropical regions, monsoons are typical atmospheric circulations with an annual reversal of low tropospheric prevailing winds and a sharp contrast between wet summers and dry winters (e.g., Webster, 1987; Trenberth et al., 2000). As phenomena of responses to the reversal of the temperature gradient between continents and adjacent oceans, monsoons are associated with the asymmetric heating of land and ocean and essentially follow the annual cycle of the solar zenith angle. Regional monsoons are interrelated, and monsoons can thus be seen as a global phenomenon. With an in-depth understanding of the variation of regional monsoons, the concept of the global monsoon has been developed (Webster et al., 1998; Trenberth et al., 2000; Wang et al., 2014; An et al., 2015) and applied to explore climate variability across multiple timescales (Liu et al., 2009; Cheng et al., 2012; Wang et al., 2012a; Wang et al., 2017), from the present-day and future (Wang and Ding, 2008; Wang et al., 2012a; Lee and Wang, 2014) to the past (Liu et al., 2009; Wang, 2009; Cheng et al., 2012; Liu et al., 2013; Jiang et al., 2015a, 2015b).

The mid-Piacenzian warm period (approximately 3.3–3.0 Ma) is an important period for understanding the near future potentially warmer world since they share with relatively unchanged paleogeography and similar Earth's physical characteristics (Salzmann et al., 2008; Dowsett et al., 2010; Haywood et al., 2016), and attracts efforts from both paleoenvironment reconstructions and paleoclimate simulations over the past two decades (e.g., Chandler et al., 1994; Sloan et al., 1996; Thompson and Fleming, 1996; Jiang et al., 2005; Salzmann et al., 2008; Dowsett et al., 2010; Lunt et al., 2010). This period is characterized by a temperature 1.9–3.6 °C above the pre-industrial period (Haywood et al., 2010, 2013, 2016), a similar greenhouse gas concentration to today (equivalent to a CO_2 concentration of approximately 405 ppmv), a sea level 22 ± 10 m above the modern state (Miller et al., 2012), warmer sea surface temperatures (Dowsett et al., 2010), seasonally free sea ice in the Arctic Ocean (Cronin et al., 1993; Robinson, 2009), a reduced ice volume due to the loss of the West Antarctic and Greenland ice sheets, and a poleward shift of vegetation belts (Salzmann et al., 2008; Dowsett et al., 2010). The mid-Piacenzian is one of the important periods for understanding the near future warming scenario

* Corresponding author.
E-mail address: jiangdb@mail.iap.ac.cn (D. Jiang).

https://doi.org/10.1016/j.palaeo.2018.06.027
Received 10 March 2018; Received in revised form 7 June 2018; Accepted 14 June 2018
Available online 21 June 2018
0031-0182/ © 2018 Elsevier B.V. All rights reserved.

(Lunt et al., 2012, 2013; Haywood et al., 2016). Investigating the behaviors and dynamics of the mid-Piacenzian global land monsoon would benefit the understanding of future monsoon change.

On geological timescales, the mid-Piacenzian monsoon is also hypothesized to play a key role in climate feedback through its impact on the carbon cycle. Several geological evidences support an enhanced Asian monsoon in the warm Pliocene (e.g., Ding et al., 1999, 2001, 2005; Yang and Ding, 2001; Rao et al., 2008; Xiong et al., 2010; Wan et al., 2012). Increased Asian monsoon precipitation would enhance physical erosion and silicate chemical weathering in Himalayan-Tibetan regions and increase organic carbon burial in marginal sea, which together contribute to the consumption of atmospheric CO_2 (France-Lanord and Derry, 1997; Galy et al., 2007, 2015; Zhang et al., 2009). Ultimately, under the decreased atmospheric CO_2, triggered by orbital configurations, the sustained major Northern Hemisphere continental glaciations developed (Lunt et al., 2008; Zhang et al., 2009), and the global climate evolved into the present bipolar glaciated state with the glacial–interglacial cycle.

Understanding the mid-Piacenzian monsoon change is crucial to test these hypotheses. However, our understanding of that issue has several limitations. The mid-Piacenzian monsoon evolution has been reconstructed by scattered and inhomogeneous geological archives from local sites. The spatial distribution of proxy data is rather sparse and uneven, thus yielding the risk of recording local signals rather than regional ones, and their representativeness on a large regional scale requires re-evaluation. Further, previous studies of monsoon evolution on geological timescales are mainly based on proxies linked to monsoon precipitation, such as chemical and magnetic indicators of soil/sediment weathering intensity (e.g., Ding et al., 1999, 2001; Yang and Ding, 2001; Sun et al., 2010; Xiong et al., 2010; Nie et al., 2014; Ao et al., 2016) and vegetation condition (e.g., Wu et al., 2007; Miao et al., 2013). However, nearly all of those proposed proxies cannot be strictly served as direct indicators of past summer monsoon intensity because those proxies also archive the combined impacts from other non-monsoon processes. The effectiveness of those summer monsoon proxies should be further examined. In addition, previous hypotheses highlight the role of Asian monsoon on the carbon cycle but not take into consideration the effect of other monsoon regions.

Based on the context provided by paleoclimate archives, paleoclimate modeling helps sharpen the interpretation of geological data and diagnose the underlying mechanisms (Schmidt, 2010; Schmidt et al., 2014; Harrison et al., 2016). Under the framework of the Pliocene Model Intercomparison Project phase 1 (PlioMIP1) (Haywood et al., 2010, 2011), coordinated simulations of the mid-Piacenzian climate from various models have been conducted (references listed in Table 1). Note that several modeling works have been performed on the mid-Piacenzian monsoons, although they only address the regional East Asian monsoon (Zhang et al., 2013; Sun et al., 2016) and the hydrological aspect of North African climate (e.g., Contoux et al., 2013; Pound et al., 2014). The mid-Piacenzian land monsoon area, precipitation, and intensity need to be investigated on a global scale, and the combination of geological evidence and simulations would give us a comprehensive picture of global land monsoon change.

Based on the above, this study focuses on the mid-Piacenzian global land monsoon variation and discusses its potential impact on climate evolution in the context of the geological timescale. We first present the outlined features of the mid-Piacenzian global land monsoon and then conduct a dynamic mechanism analysis and model–data comparison, aiming to understand the potential role of monsoon evolution on the carbon cycle and even the onset of major Northern Hemisphere glaciations.

2. Data and methods

2.1. Models and PlioMIP1 experimental design

Experiments of 14 climate models for the mid-Piacenzian with available data have been applied here to investigate monsoon mechanism (here we do not include the experiments of MRI-CGCM2.3-AGCM and MRI-CGCM2.3 because of the absence of vertical geopotential height data necessary for diagnosing deep tropospheric dynamics), including six atmospheric general circulation models (AGCMs) and eight fully coupled atmosphere–ocean general circulation models (AOGCMs). According to the experimental design of the PlioMIP1 (Haywood et al., 2010, 2011), each model performs both a pre-industrial and a mid-Piacenzian simulation. In the pre-industrial simulations, the atmospheric concentrations of CO_2 and CH_4 are set to 280 ppmv and 760 ppbv, respectively. In the mid-Piacenzian simulations, reconstructed ice-sheet and vegetation by PRISM3D (versions of the Pliocene Research Interpretation and Synoptic Mapping boundary condition data sets) are imposed; a reconstructed topography is guided to add to the model; the atmospheric CO_2 concentration is fixed at 405 ppmv; and the orbital parameters and solar constant are set to the pre-industrial levels. In addition, the reconstructed climatologic monthly sea surface temperatures are used in the AGCM simulations. There are two boundary condition data packages, provided by PRISM and utilized by PlioMIP1, with the preferred package used for models that can change the land–sea mask into a mid-Piacenzian configuration and the alternate one for models that face difficulty in land–sea mask modification (Dowsett, 2007; Robinson et al., 2008; Salzmann et al., 2008, 2009; Dowsett and Robinson, 2009; Dowsett et al., 2009; Sohl et al., 2009; Haywood et al., 2010, 2011). Basic information on climate models and data is outlined in Table 1, and further details of the specific model experimental design can be found in the references listed in Table 1. The long-term mean precipitation climatology of version–2.2 Global Precipitation Climatology Project monthly reanalysis data (hereafter referred to as “GPCP observation”; Adler et al., 2003; Huffman et al., 2009) and of Climate Prediction Center merged analysis (hereafter referred to as “CMAP observation”; Xie and Arkin, 1997) for the period 1981–2010 are used to assess the model performance. To capture the variation of monsoon area in details, both the model data and observations are aggregated to a horizontal resolution of 2.5° latitude by 2.5° longitude through bilinear interpolation (we aggregate the relatively high resolution CCSM4 data through conservative interpolation). According to the availability of specific humidity and vertical zonal and meridional wind data, we only calculate the ensemble means of three AGCMs (CAM3.1, CAM4, and MIROC4m-AGCM), four AOGCMs (CCSM4, FGOALS-g2, MIROC4m, and NorESM-L), and all these seven models to provide the information of the vertically integrated water vapor flux. For the moisture budget analysis, only four models (CAM3.1, CAM4, FGOALS-g2, and NorESM-L) are calculated because of the unavailability of vertical velocity or specific humidity data for other models.

2.2. Definitions of global land monsoon domain, precipitation, and precipitation intensity

The monsoon climate is best characterized by the reversed prevailing surface wind during contrasting wet summers and dry winters. Coordinated by the annual cycle of solar heating, the temperature gradients between continental regions and adjacent oceans reverse seasonally. Consequently, warm and moist summer winds blow inland from the oceans during rainy season, whereas cool and dry winter air flow reverses from the hearts of the continents during the dry season (Webster, 1987; Trenberth et al., 2000). Following previous studies (Wang and Ding, 2008; Wang et al., 2012a), the global land monsoon area (GLMA) is identified by two criteria: the annual precipitation range (local summer–minus–winter mean precipitation rate) goes beyond 2 mm day^{-1}, and the ratio of local summer precipitation to annual total precipitation exceeds 55%. The boreal summer (austral winter) consists of May, June, July, August, and September (MJJAS), and the boreal winter (austral summer) consists of November, December, January, February, and March (NDJFM). The modern climatological GLMA, as expressed by GPCP or CMAP observations, is composed of six major regional monsoons of northern Africa, Asia, North America, southern Africa, Australia, and South America and shares a similar spatial pattern to those obtained by Liu et al. (2009) and Wang et al. (2012a). According to Hsu et al. (2012) and Wang et al. (2012a), the global land monsoon precipitation (GLMP) is defined as the sum of total summer precipitation in the GLMA, and the global land monsoon precipitation intensity (GLMPI) is measured by the area-weighted summer precipitation in the GLMA.

Table 1
Basic information about the models used in this study.

Model ID		Boundary conditions	Atmospheric resolution	Years used for analysis	Reference
Six atmospheric models					
1	CAM3.1	Alternate	~2.8° × 2.8°, L26	30	Yan et al. (2012)
2	CAM4	Alternate	3.75° × 3.75°, L26	20	Zhang and Yan (2012)
3	ECHAM5	Preferred	3.75° × 3.75°, L19	30	Stepanek and Lohmann (2012)
4	HadAM3	Preferred	2.5° × 3.75°, L19	30	Bragg et al. (2012)
5	LMDZ5A	Alternate	~1.9° × 3.75°, L39	30	Contoux et al. (2012)
6	MIROC4m-AGCM	Preferred	~2.8° × 2.8°, L20	30	Chan et al. (2011)
Eight coupled atmosphere–ocean models					
7	CCSM4	Alternate	~0.9° × 1.25°, L26	30	Rosenbloom et al. (2013)
8	COSMOS	Preferred	3.75° × 3.75°, L19	30	Stepanek and Lohmann (2012)
9	FGOALS-g2	Alternate	~2.8° × 3–6°, L26	30	Zheng et al. (2013)
10	GISS-E2-R	Preferred	2° × 2.5°, L40	30	Chandler et al. (2013)
11	HadCM3	Alternate	2.5° × 3.75°, L19	50	Bragg et al. (2012)
12	IPSLCM5A	Alternate	~1.9° × 3.75°, L39	30	Contoux et al. (2012)
13	MIROC4m	Preferred	~2.8° × 2.8°, L20	30	Chan et al. (2011)
14	NorESM-L	Alternate	3.75° × 3.75°, L26	200	Zhang et al. (2012)

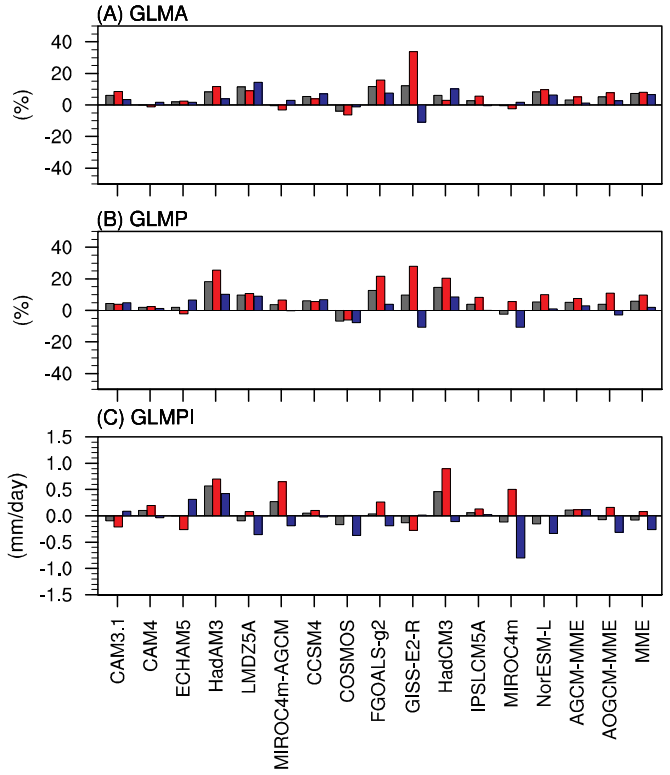

Fig. 1. Percentage changes of global land monsoon areas (A, GLMA) and monsoon precipitation (B, GLMP), and change of GLMP intensity (C, GLMPI; units: mm day^{-1}) in the mid-Piacenzian relative to the pre-industrial period. The gray, red, and blue bars represent the global, northern and southern hemispheric land domains, respectively. For the multi-model ensemble means, we firstly obtain the monsoon areas in the mid-Piacenzian and the pre-industrial periods based on multi-model ensemble mean precipitation, and then calculate the percentage changes of GLMA, GLMP, and GLMPI. (For interpretation of the references to colour in this figure legend, the reader is referred to the web version of this article.)

2.3. Evaluation of PlioMIP1 models

Because the criteria of land monsoon area are based on precipitation, it is necessary to evaluate the ability of climate models in simulating the annual, summer, and winter precipitation climatology in land monsoon domains, because such a capacity is directly related to the confidence of the simulations. Both observations and simulations show that almost all of the land monsoon domains locate at 40°S–70°N, where the spatial correlation coefficients, normalized standard deviation, and normalized centered root-mean-square error of each pre-industrial experiment against the observations are calculated individually and shown in a Taylor diagram (Fig. S1). The three statistical variables for the annual (MJJAS and NDJFM) precipitation are, in order, 0.67–0.86 (0.68–0.85 and 0.68–0.87), 0.95–1.26 (0.97–1.17 and 0.95–1.26), and 0.54–0.88 (0.56–0.88 and 0.54–0.86) when using GPCP observations to evaluate the models and are 0.72–0.88 (0.71–0.86 and 0.72–0.88), 0.86–1.13 (0.89–1.07 and 0.89–1.17), and 0.48–0.76 (0.52–0.79 and 0.50–0.77) when using CMAP observations to evaluate the models. Both evaluations indicate a reasonable ability of climate models on the spatial pattern and variability of the observed precipitation climatology, although there is a level of dependence to the observation. As such, it is not necessary to exclude any model. The Taylor diagram shows that the ensemble means of six AGCMs, eight AOGCMs, and all 14 models (hereafter referred to as "AGCM-MME", "AOGCM-MME", and "MME", respectively) have higher reliability than do most of individual models and are thus emphasized in our analysis.

3. Mid-Piacenzian global land monsoon change

3.1. Mid-Piacenzian changes of GLMA, GLMP, and GLMPI

Compared to the pre-industrial period, the mid-Piacenzian GLMA increases in most models and by an average of 7.3% or 3.2×10^6 km^2 (Fig. 1A). The land monsoon area expands in both the Northern and Southern Hemispheres in most models at an average rate of 7.9% and 6.5%, respectively. Although there is some spread among the models, the results of the AGCM-MME and AOGCM-MME are generally consistent with those of the MME (Fig. 1A). Spatially, the ensemble means indicate that most of land monsoon areas expand poleward (Fig. 2), which is characteristic in all individual models except COSMOS (Fig. S2). On the regional scale, the mid-Piacenzian land monsoon domains increase in northern Africa (15.1%), Asia (10.5%), and northern Australia (48.3%), decrease in North America (−27.1%), and vary slightly in southern Africa (−2.3%) and South America (2.5%). Taken together, the mid-Piacenzian GLMA expands, which is mainly derived from the expanded domains in northern Africa, Asia, and northern Australia.

The criteria used to define the monsoon areas, including the area-averaged annual precipitation range (summer minus winter), summer precipitation, and annual precipitation over the domains where the mid-Piacenzian monsoon area varies relative to the pre-industrial period, are calculated to investigate the reason of GLMA change (Fig. S3). At the global scale, the summer and annual precipitation over land monsoon domains increases on average by 0.49 mm day^{-1} and 0.33 mm day^{-1}, respectively. Consequently, the ratio of summer to annual precipitation increases as a result of the larger increase for the former than the latter. Additionally, the

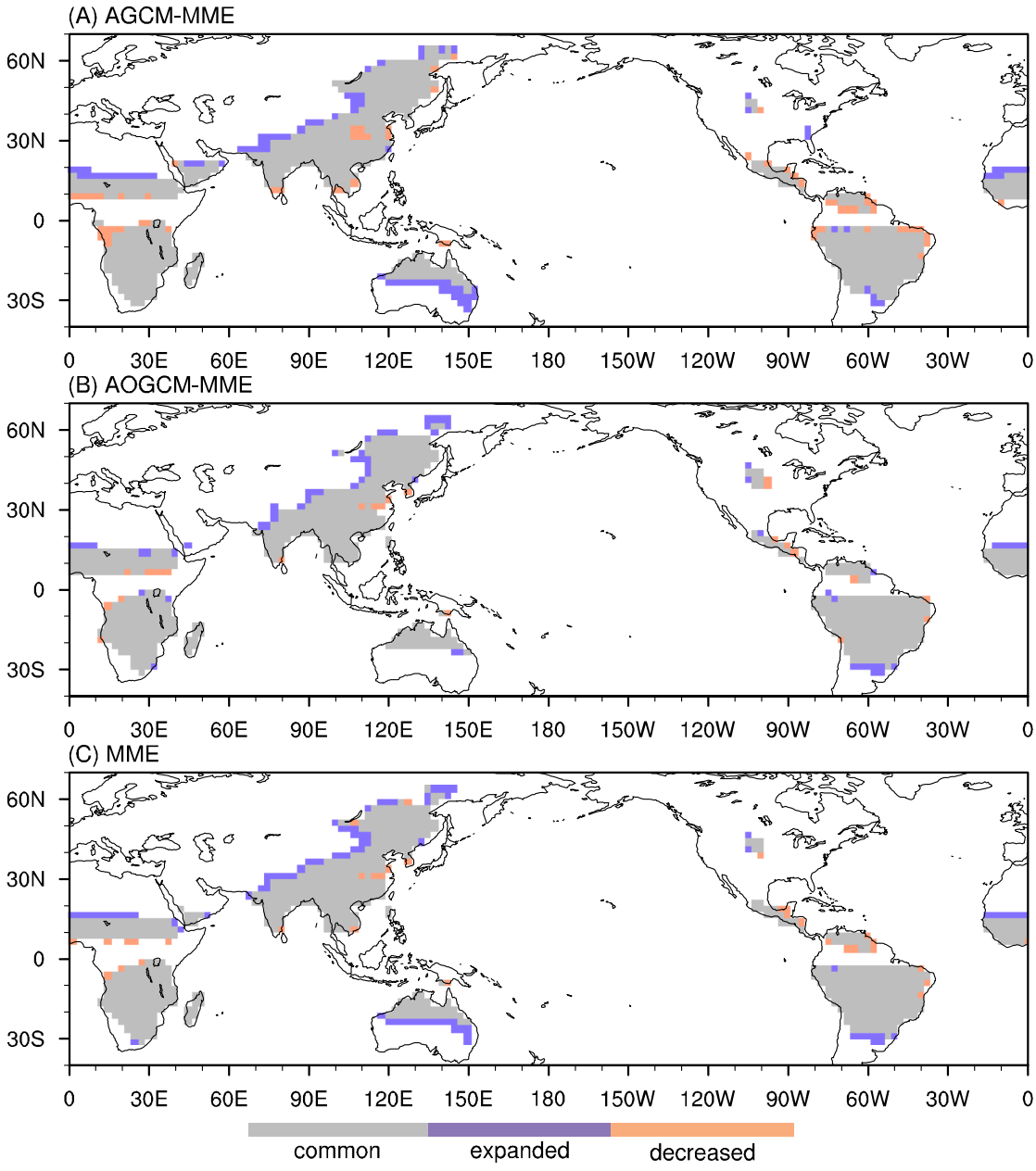

Fig. 2. Global land monsoon domains from the ensemble mean of (A) AGCMs, (B) AOGCMs, and (C) all 14 models. Light blue (orange) shadings indicate the expanded (decreased) domains in the mid-Piacenzian compared with the pre-industrial period, and gray indicates the common monsoon domains between them. (For interpretation of the references to colour in this figure legend, the reader is referred to the web version of this article.)

annual range is augmented by an average of 0.34 mm day^{-1}. Thus, both the increased ratio of summer to annual precipitation and the augmented annual range contribute to the mid-Piacenzian GLMA expansion.

Compared with the pre-industrial period, the mid-Piacenzian GLMP increased in most models and by an average of 5.8% or 14.7×10^9 m^3 day^{-1} (Fig. 1B). For the spatial distribution (Fig. 3), land monsoon precipitation generally increased in northern Africa, Asia, northern Australia, and western South America but decreased in North America and eastern South America. The land monsoon precipitation increased in both the Northern and Southern Hemispheres, with average rates of 9.6% and 2.1%, respectively. Regionally, more land monsoon precipitation occurs in northern Africa (22.5%), Asia (14.0%), and northern Australia (56.0%), less occurs in North America (−36.1%), and little variation occurs in southern Africa (−2.2%) and South America (−2.0%). Overall, the increased GLMP comes mainly from northern Africa, Asia, and northern Australia.

The MME results indicate that the mid-Piacenzian GLMPI varies by −0.08 mm day^{-1} (−1.4%), with an increase in the Northern Hemisphere (by 0.08 mm day^{-1}) and a decrease in the Southern Hemisphere (by −0.26 mm day^{-1}) (Fig. 1C). For the local land monsoon domains, the mid-Piacenzian monsoon precipitation intensifies in northern Africa (6.4%), Asia (3.1%), southern Africa (0.09%), and northern Australia (5.2%) but weakens in North America (−12.2%) and South America (−4.4%).

The mid-Piacenzian changes in GLMA and GLMPI are further analyzed to understand the GLMP variation. As shown in Supplementary Fig. S4, the decreased (increased) GLMP is consistently simulated as having reduced (expanded) GLMA by most models. The GLMP variation generally follows a positive relationship with the GLMA change, with a coefficient of determination of 0.60 (statistically significant at the 95% confidence level) for all models. To detect the role of GLMA and GLMPI variations, the mid-Piacenzian GLMP variation is decomposed into three items; the monsoon precipitation variations in the mid-Piacenzian expanded monsoon domains,

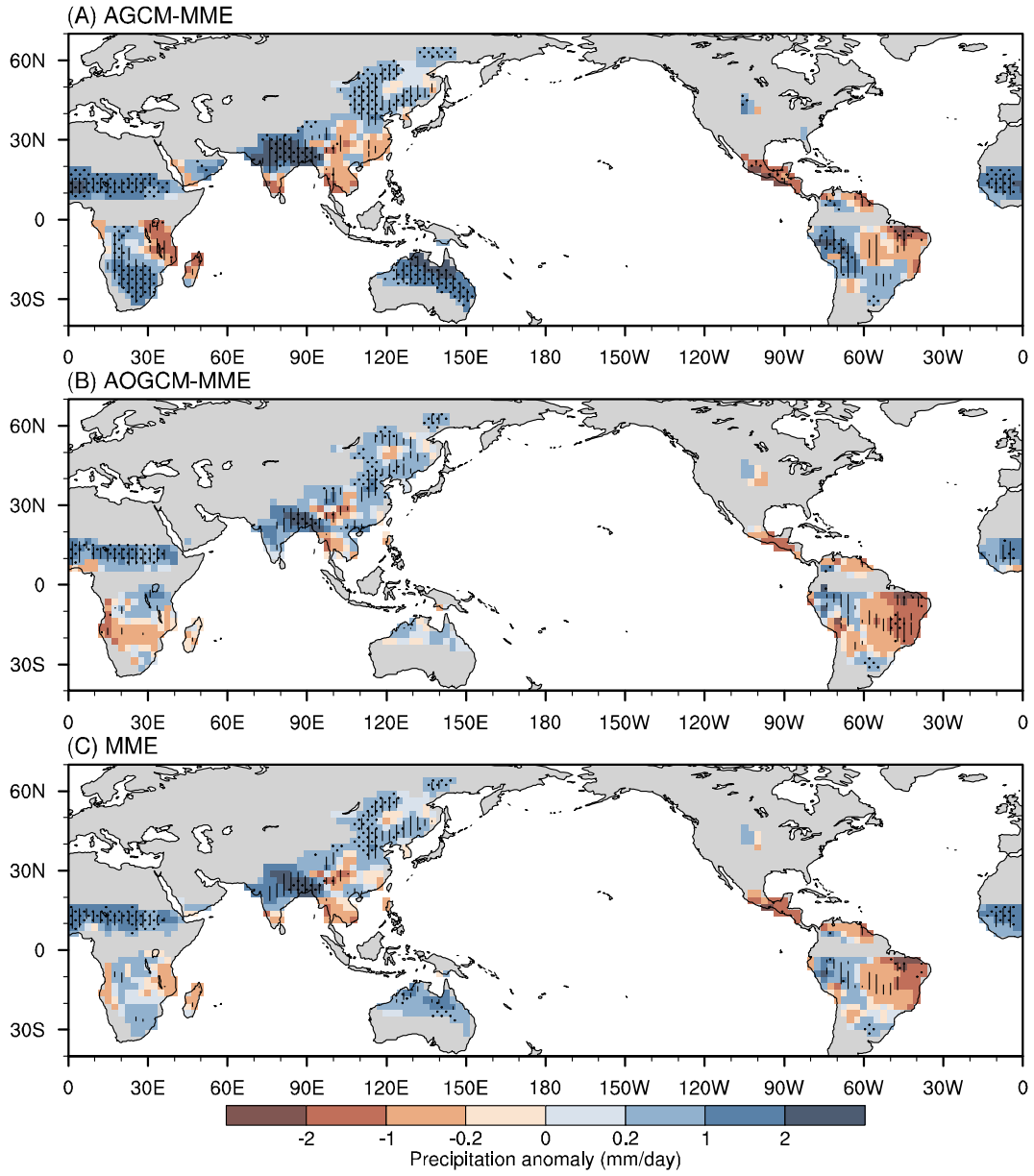

Fig. 3. Anomaly of summer precipitation in the mid-Piacenzian relative to the pre-industrial period over the land monsoon domains shown in Fig. 2 from the ensemble mean of (A) AGCMs, (B) AOGCMs, and (C) all 14 models. In panels (A) to (C), the summer precipitation stands for May–September (November–March) precipitation in the northern (southern) hemisphere (shading, units: mm day^{-1}). The hatched areas represent regions where more than 75% of the models simulate a consistent signal, and the dots indicate regions where the absolute value of the multi-model mean anomaly is larger than one standard deviation of the models. (For interpretation of the references to colour in this figure legend, the reader is referred to the web version of this article.)

in decreased monsoon domains, and in common monsoon domains between two periods (see Supplementary Formula 1). For all models, the magnitudes of GLMPI-induced monsoon precipitation variations in the common monsoon domains are clearly smaller than the magnitudes of monsoon precipitation variations induced by GLMA variations in expanded and decreased monsoon domains (Formula S1 and Fig. S5). Hence, it is the variation of GLMA, rather than of GLMPI, that plays the major role in the GLMP change.

3.2. Dynamic mechanism for changes of the mid-Piacenzian monsoon area and precipitation

As a deep tropospheric overturning circulation system, monsoon varies largely with the deep tropospheric thermal gradient (Li and Yanai, 1996; Ueda et al., 2006; Dai et al., 2013). The deep tropospheric temperature gradient corresponds to horizontal gradient of mid-to-upper tropospheric thickness (e.g., Dai et al., 2013). Since most models provide vertical wind data but few provide vertical temperature data, here we use the tropospheric layer thickness (between 200 hPa and 500 hPa levels), instead of the layer-mean temperature, to discuss the thermal contrasts.

In the Northern Hemisphere, the summer tropical warming pattern (represented by mid-upper tropospheric thickness change in Fig. 4) features stronger warming at mid-latitudes than at low latitudes, forming an anomalous relatively high pressure in low-latitude Asian region (Fig. S6). The correspondingly augmented meridional pressure gradient in East Asia contributes to the anomalous low-level southerly winds (Fig. S6 and also Fig. 5 in Zhang et al., 2013) and northward moisture transport from tropical ocean (Fig. 5). In the meantime, anomalous anticyclones (cyclones) in the upper level located in subtropical Asia and northern Africa (tropical North America) (Fig. 4) are favorable for large-scale ascent and convective

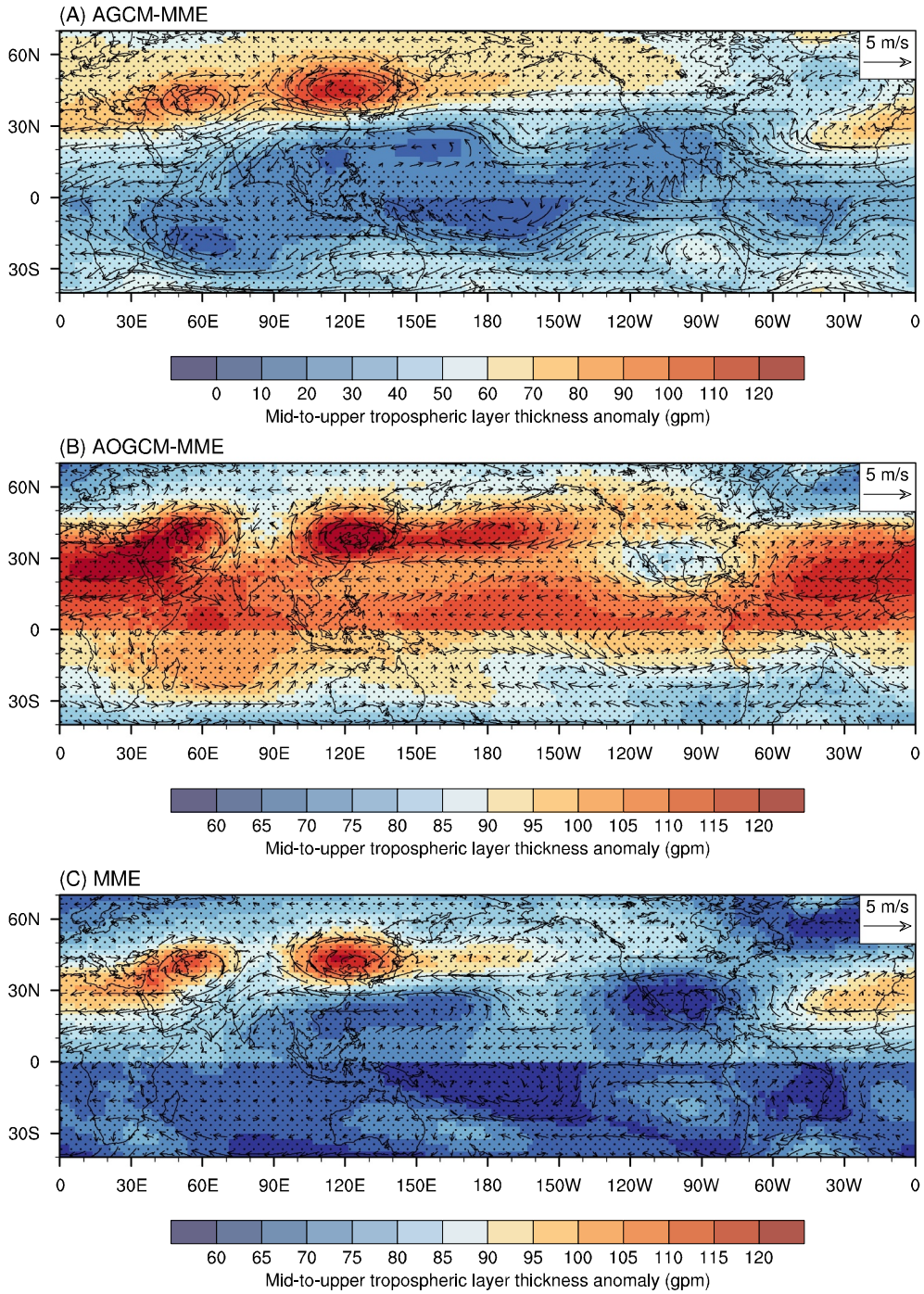
(A) AGCM-MME
5 m/s
60N
30N
0
30S
0 30E 60E 90E 120E 150E 180 150W 120W 90W 60W 30W 0
0 10 20 30 40 50 60 70 80 90 100 110 120
Mid-to-upper tropospheric layer thickness anomaly (gpm)
(B) AOGCM-MME
5 m/s
60N
30N
0
30S
0 30E 60E 90E 120E 150E 180 150W 120W 90W 60W 30W 0
60 65 70 75 80 85 90 95 100 105 110 115 120
Mid-to-upper tropospheric layer thickness anomaly (gpm)
(C) MME
5 m/s
60N
30N
0
30S
0 30E 60E 90E 120E 150E 180 150W 120W 90W 60W 30W 0
60 65 70 75 80 85 90 95 100 105 110 115 120
Mid-to-upper tropospheric layer thickness anomaly (gpm)

Fig. 4. Anomaly of the summer tropospheric layer thickness (between 200 and 500 hPa levels, shading, units: gpm) and wind (vector, 200 hPa, units: m s^{-1}) in the mid-Piacenzian relative to the pre-industrial period, from the ensemble mean of (A) AGCMs, (B) AOGCMs, and (C) all 14 models. The summer stands for May–September (November–March) in the northern (southern) hemisphere. The black dots indicate regions where the absolute value of the multi-model mean anomaly is larger than one standard deviation of the models. (For interpretation of the references to colour in this figure legend, the reader is referred to the web version of this article.)

(descent and diffusive) flow, as identified by the anomalous upper-tropospheric divergence (convergence) with negative (positive) 200 hPa velocity potential (Fig. 6). As a result, the Asian and northern African land monsoon precipitation increases and North American monsoon precipitation reduces. In contrast to other models, COSMOS simulates a less warming rate in Asian land monsoon domain relative to surrounding regions in the mid-Piacenzian (Fig. S7). The anomalous thermal contrast from COSMOS favors large-scale descent flow in the Asian land monsoon domain, as identified by the anomalous upper-tropospheric convergence with positive 200 hPa velocity potential (Fig. S8). The thermal contrast change explains largely why COSMOS simulates a widely decreased monsoon precipitation in the Asian land monsoon domain.

In the Southern Hemisphere during boreal winter, averaged over all models (Fig. 4C), anomalous warming (represented by mid-upper tropospheric thickness change) in southern Africa, northern Australia, and western South America is slightly greater than that of surrounding regions. Anomalous upper lever wind divergences occur in those regions with negative 200 hPa velocity potential (Fig. 6), which benefits anomalous upward motions. Contrary conditions occur in eastern South America with anomalous downward motions indicated by upper wind convergence with positive 200 hPa velocity potential (Fig. 6). The increased (decreased) water vapor convergence covers the regions of southern Africa, northern Australia, and western South America (eastern South America) (Fig. 5), where the monsoon precipitation increases (decreases) (Fig. 3).

The moisture budget analysis indicates that changes in vertical moisture advection and the evaporation explain most precipitation increase (decrease) in expanded (decreased) monsoon domains. Most monsoon precipitation changes in expanded and decreased monsoon domains come

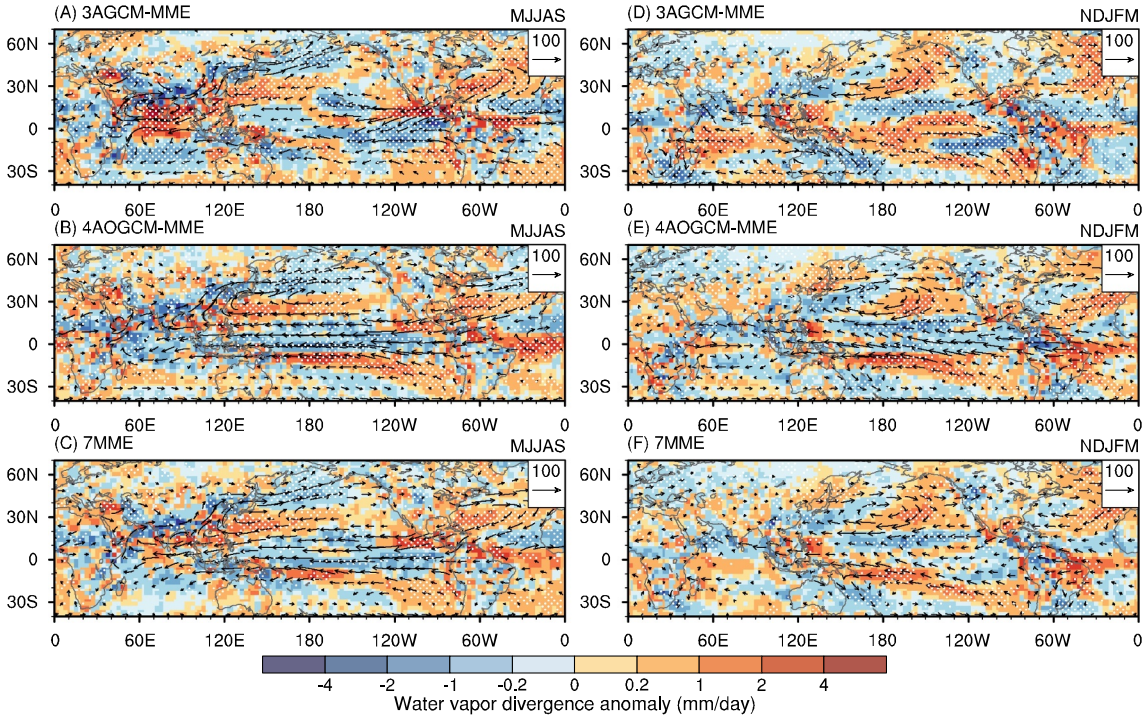

Fig. 5. Anomaly of vertically integrated water vapor flux (arrows, units: kg m^{-1} s^{-1}) and its divergence (shading, units: mm day^{-1}) in the mid-Piacenzian relative to the pre-industrial period for (A, B, and C) the May–September, and (D, E, and F) November–March. Water vapor flux lower than 10 kg m^{-1} s^{-1} is not shown. According to the availability of specific humidity and wind data, here we only calculate the ensemble means of three AGCMs (CAM3.1, CAM4, and MIROC4m-AGCM), four AOGCMs (CCSM4, FGOALS-g2, MIROC4m, and NorESM-L), and all these seven models. The vertical integration is performed from the surface to 100 hPa. The white dots indicate regions where the absolute value of the multi-model mean anomaly is larger than one standard deviation of the models. (For interpretation of the references to colour in this figure legend, the reader is referred to the web version of this article.)

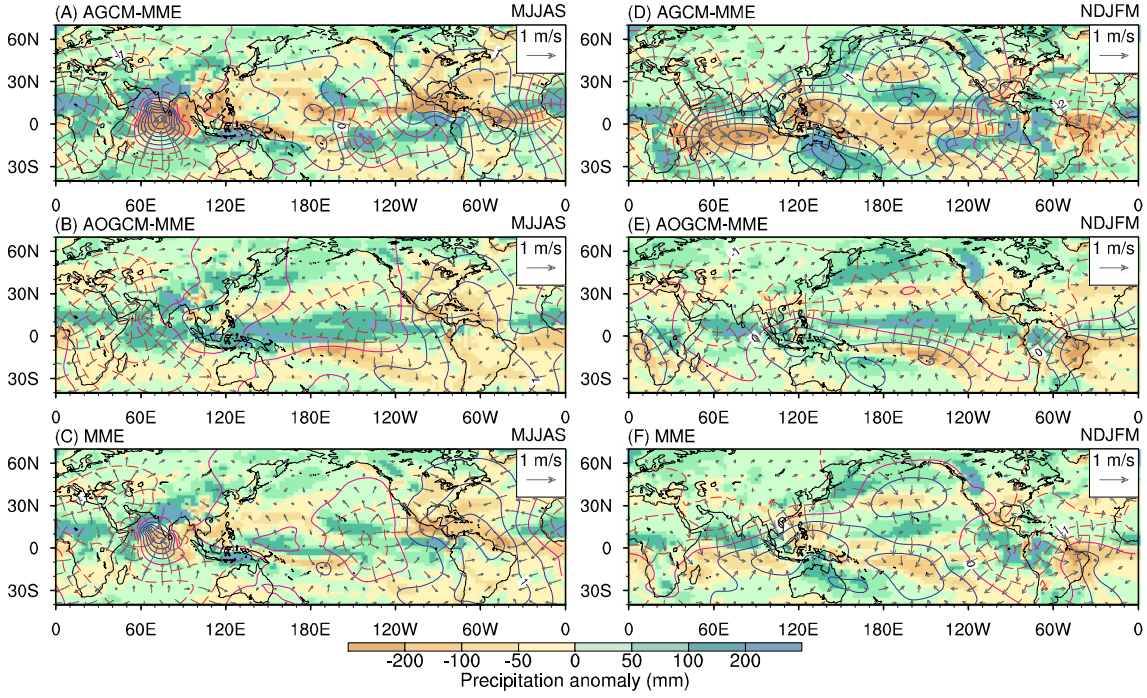

Fig. 6. Anomaly of the boreal summer (May–September, left panels) and austral summer (November–March, right panels) precipitation (shading, units: mm), 200 hPa velocity potential (contour, χ, interval 0.5 × 10^6 m^2 s^{-1}), and 200 hPa divergent wind (vector, m s^{-1}) in the mid-Piacenzian relative to the pre-industrial period as derived from the ensemble mean of (A and D) AGCMs, (B and E) AOGCMs, and (C and F) all 14 models. (For interpretation of the references to colour in this figure legend, the reader is referred to the web version of this article.)

firstly from the change in vertical moisture advection and secondly from the evaporation change (Fig. 7). The vertical moisture advection could be mainly divided into the dynamic and thermodynamic components, which are associated with vertical motion and water vapor, respectively (Chou and Lan, 2012; Chou et al., 2013). The dynamic component of vertical moisture advection change, with positive values in the expanded monsoon domains but negative ones in the decreased monsoon domains, dominates the changes of vertical moisture advection in those regions (Fig. 8).

Overall, in the mid-Piacenzian, anomalous inland water vapor transport induced by the reduced meridional thermal contrast, together with increases in vertical moisture advection and the evaporation, mostly explained the increased GLMP and the varied GLMA.

3.3. Inter-model comparison

The AGCM-MME and AOGCM-MME consistently simulate more monsoon precipitation over northern Africa, the northern parts of Southern Asia and East Asia, northern Australia, and western South America, and less monsoon precipitation in North America and eastern South America (Fig. 3). There are also disagreements between the two types of ensemble averages. First, the signal of monsoon precipitation variation is opposite in some regions. This is particularly obvious in the southern part of South Asia where monsoon precipitation decreases in the AGCM-MME but increases in the AOGCM-MME. Second, the magnitude of monsoon precipitation variation is different in monsoon domains of northern Africa, northern Southern Asia, and northern Australia, where the monsoon precipitation increases more in the AGCM-MME than in the AOGCM-MME.

At the same time, it is obvious that summer tropical circulation change between AGCM-MME and AOGCM-MME is different in some regions (Fig. 6). More specifically, the AGCM-MME simulates an anomalous upper-tropospheric convergence in tropical Indian Ocean (positive 200 hPa velocity potential), indicating large-scale descent and divergent outflow. By contrast, the AOGCM-MME simulates an anomalous upper-tropospheric divergence in western tropical Indian Ocean (negative 200 hPa velocity potential), indicating large-scale ascent and convective outflow. Hence the AGCM-MME simulates a drier summer condition over southern part of South Asia while the AOGCM-MME simulates a wetter one. Besides, the magnitude of anomalous upper-tropospheric divergences over the northern Africa and northern Australia simulated by AGCM-MME is larger than that simulated by AOGCM-MME, indicating stronger ascent motions and thus more precipitation there in the mid-Piacenzian. Such differences in tropical circulation changes between the two model groups reflect the different behaviors of Walker circulation in the mid-Pliocene simulated by them (Corvec and Fletcher, 2017). The AGCMs simulate overall weakened Walker circulation driven by an increasing atmospheric stability. By contrast, the AOGCMs simulate less weakening of the Walker circulation. The patterns of sea surface temperature simulated by AOGCMs differ from the prescribed one in AGCMs, which is thought to be the underlying factor of the different tropical circulation change between the two model groups (Corvec and Fletcher, 2017). Considering that the spatial distribution of sea surface temperature changes is crucial to tropical circulation and thus monsoon precipitation, more accurate reconstructions of tropical sea surface temperatures are highly called for in future studies. The tropical sea surface temperature change in the mid-Piacenzian also needs to be paid attention to in the second phase of PlioMIP (PlioMIP2).

Taken together, the different magnitudes of tropical warming and the different pattern of sea surface temperature change between two types of ensemble averages explain the model disagreement between them to some degree.

4. Discussion

4.1. Model–data comparison

The geological evidence that records the continuous history of monsoon evolution since the mid-Piacenzian is rare. At present, the long sequences of geological evidence are mainly obtained from the loess–red clay sequences in the Chinese Loess Plateau and sediments in paleolakes and deep-sea (Rea, 1994; Ding et al., 1995; Liu and Ding, 1998; An et al., 2001; Guo et al., 2002; Fu et al., 2013; Ao et al., 2016). Because of the scarcity of geological evidence, the paleoenvironmental records close to the monsoon region, such as geological records in Qinghai Lake and the Qaidam Basin, near the northwest boundary of East Asian monsoon domains, have also been used in the model–data comparison. In addition, the eolian mass accumulation ratios in the North Pacific and the Atlantic are closely related to the continental aridity of the eolian source regions and have been compared with simulations as indirect evidence. All of the geological records collected here consist of two categories (Table 2): the first type indicates the wet/dry variation at and around reconstruction sites, and the second type indirectly hints at the aridity of the continental eolian source regions, mainly on the basis of the eolian mass accumulation ratios at deep-sea sites. Moreover, the summer monsoon proxies, such as chemical and magnetic indicators of weathering, vegetation conditions, mostly reflect information about climatological annual precipitation or humidity. In some ways, those proxies are reasonable for reconstructing the summer precipitation because it accounts for more than 55% of the annual total precipitation over land monsoon areas.

In general, the simulated mid-Piacenzian land monsoon area and precipitation are roughly consistent with geological evidence on both the local and regional scales (Fig. 9). For northern Africa, most of the models simulated an increased monsoon area and precipitation and a poleward expansion of the northern monsoon domain boundary (Figs. 2 and 3). Consistently, wetter conditions in northern Africa are supported by a smaller proportion of C_4 vegetation in the mid-Piacenzian than in the late Quaternary (Cerling, 1992; Wynn, 2004) and by the expansion of lake water at the time, such as Lake Chad and Lake Sudd (Schuster et al., 2009; Otero et al., 2010; Pound et al., 2014). Other geological evidence, such as eolian depositions on the deep-sea sites of ODP (Ocean Drilling Program) 659, 662/663, 664, 231, and 721/722 around northern Africa, further indirectly imply a wetter condition in the mid-Piacenzian, as illustrated by lower mass accumulation rates in the mid-Piacenzian than in the Late Quaternary (Clemens and Prell, 1990; Tiedemann et al., 1994; deMenocal, 1995; Clemens et al., 1996; Feakins et al., 2005).

Specific to Asia, all models simulated an increase in monsoon area and precipitation (Figs. 2 and 3). The simulated wetter conditions are also recorded at several sites in northwestern and northern China. The Qinghai Lake at the present monsoon marginal area exhibits higher lake levels in the mid-Piacenzian relative to the late Quaternary, as supported by evidence of lithology, mean grain size, and clay minerals in lake sediments (Fu et al., 2013; Zeng et al., 2014). The history of paleo-lake evolution in the western Qaidam Basin at the present monsoon marginal area shows a clear shrinkage trend since the late Pliocene by sedimentary carbonate, evaporite, and pollen evidence (Cai et al., 2012; Wang et al., 2012b; Miao et al., 2013; Yang et al., 2013). The paleoenvironmental reconstructions in the Chinese Loess Plateau at the present typical monsoon indicate quite higher annual precipitation by magnetic parameters (Nie et al., 2014), higher free iron oxides contents (Ding et al., 2001; Yang and Ding, 2001), high authigenic calcite $^{87}Sr/^{86}Sr$ ratios (Rao et al., 2008) and moisture loving vegetation cover by pollen analysis (Wu et al., 2007). It is noted that the Mu Us Desert nowadays as the northern margin of the Chinese Loess Plateau was located more northward in the mid-Piacenzian because the sand-sized particle content within loess near the desert margin was less than that in the late Quaternary, indicating a wetter and an expanded monsoon region in northern China (Ding et al., 1999, 2005). The simulated poleward shift or northward migration of the East Asian monsoonal domain (Fig. 2) is also confirmed by the reconstructed northerly penetration (approximately 400 km) of the monsoon rainbelt during the Pliocene warmth by the red clay sediments in northern China (Yang et al., 2018). Further, the generally wetter conditions in the Asian monsoon domain and nearby regions in the mid-Piacenzian are also supported by indirect geological evidence. The eolian depositions at the North Pacific deep-sea sites are mainly transported

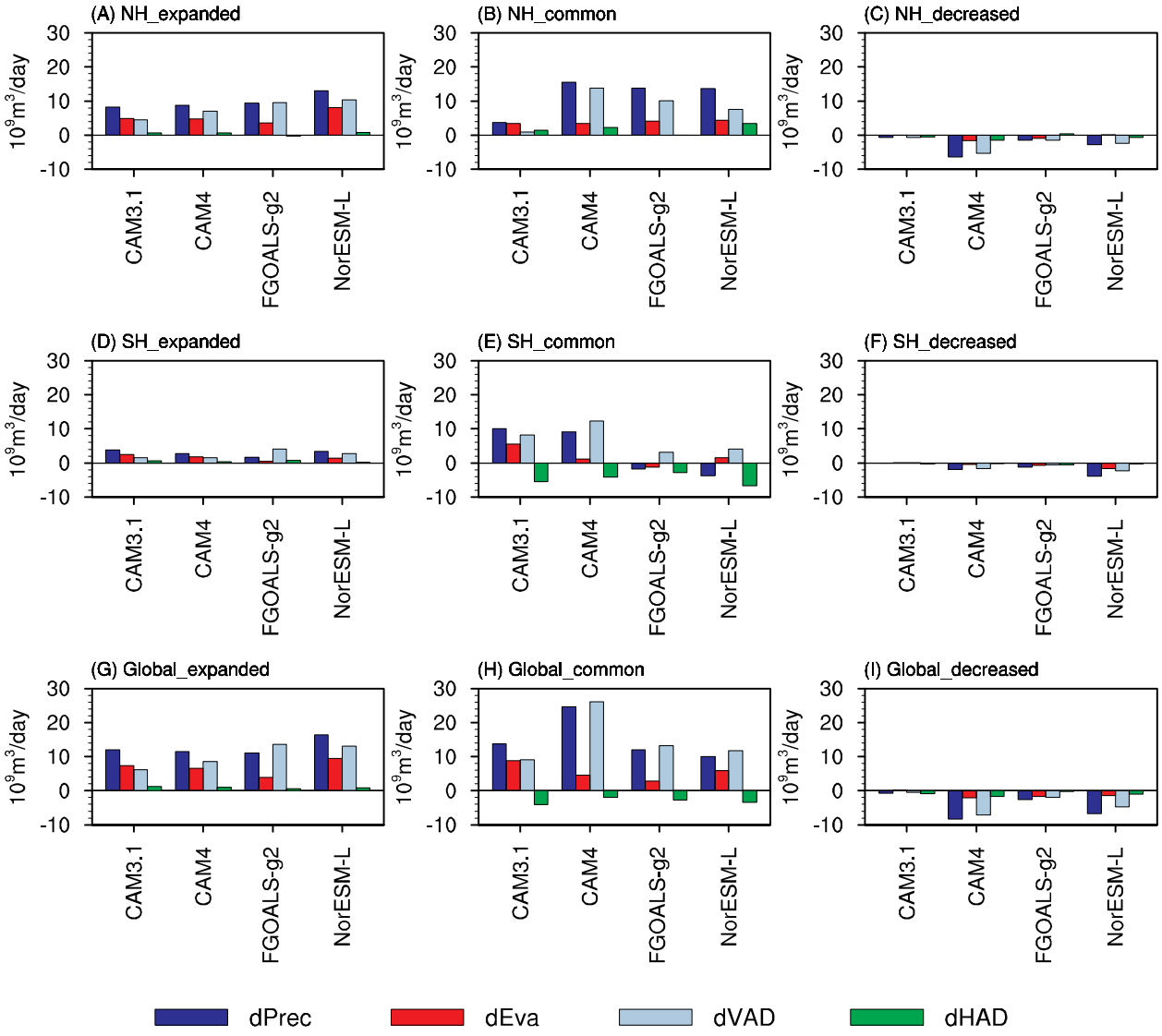

Fig. 7. Moisture budget (units: $\times 10^9\ m^3\ day^{-1}$) of land monsoon precipitation change for expanded (left panels, A, D, and G), common (middle panels, B, E, and H), and decreased (right panels, C, F, and I) monsoon domains from four model experiments in the mid-Piacenzian relative to the pre-industrial period. Results of the Northern hemisphere, Southern hemisphere, and global are shown in the upper, middle, and lower rows, respectively. Blue (red) bars indicate the precipitation (evaporation) change. Light blue (green) bars indicate the change of vertical moisture advection (horizontal moisture advection) component. The moisture budget method is shown in supplementary Formula 2. (For interpretation of the references to colour in this figure legend, the reader is referred to the web version of this article.)

from the Asian inland by zonal westerlies, and their mass accumulation rates are closely related to the aridity of the eolian source regions in Asian inland (Rea, 1994), with higher rates indicating greater aridity. The eolian mass accumulation rate of ODP sites 885/886 yields rather smaller values in the mid-Piacenzian than those in the late Quaternary, indicating wetter conditions in the Asian inland at the time (Rea and Leinen, 1988; Rea et al., 1998). Moreover, the decline of mass accumulation rates of eolian depositions on the central Chinese Loess Plateau supports a less pronounced Asian interior aridity in the mid-Piacenzian (Sun and An, 2005). The above all evidence indicates wetter conditions in the Asian inland and northern East Asian monsoon regions and agrees with the simulations. In addition, the consistent model–data comparison in Asia could also be tested in the Yunnan region at the present south Asian monsoon area. The late Pliocene climate parameters in western Yunnan reconstructed through the coexistence approach to palynological data showed that the annual precipitation slightly reduces in Eryuan (Kou et al., 2006), slightly increases in Yangyi, and extremely decreases in Longling. Considering the uncertainty of the coexistence method used in their study, the variation in Eryuan and Yangyi might lie in the range of biases. Thus, the extreme reduction signal in Longling is relatively robust, as supported by the reduced monsoon precipitation simulated by multi-model ensemble means (Fig. 9).

For the remaining land monsoon domains, the reconstructed northward extension of forests, woodlands and savannah into the present arid regions during the Pliocene supports the simulated northward shift of the West African monsoon during the Pliocene (Salzmann et al., 2008; Vallé et al., 2014). Paleobotany research reveals that grassland is prominent in central northern Australia in the late Pliocene, and that the climatic regime is substantially wetter than that of the present day (Martin, 2006), consistent with the simulated increased monsoon precipitation in most Australia. In Central America, paleobotany evidence indicates that the tropical rain forest is absent or poorly represented in southeastern Guatemala (Graham, 1998) and that the annual precipitation in southeastern Costa Rica is estimated at near the present level (Graham and Dilcher, 1998). Additionally, the reconstructed drier condition in southeastern Guatemala agrees with the simulated monsoon precipitation deficit. As to eastern South America, reconstructed paleobiogeography shows an expanded savanna-grasslands area

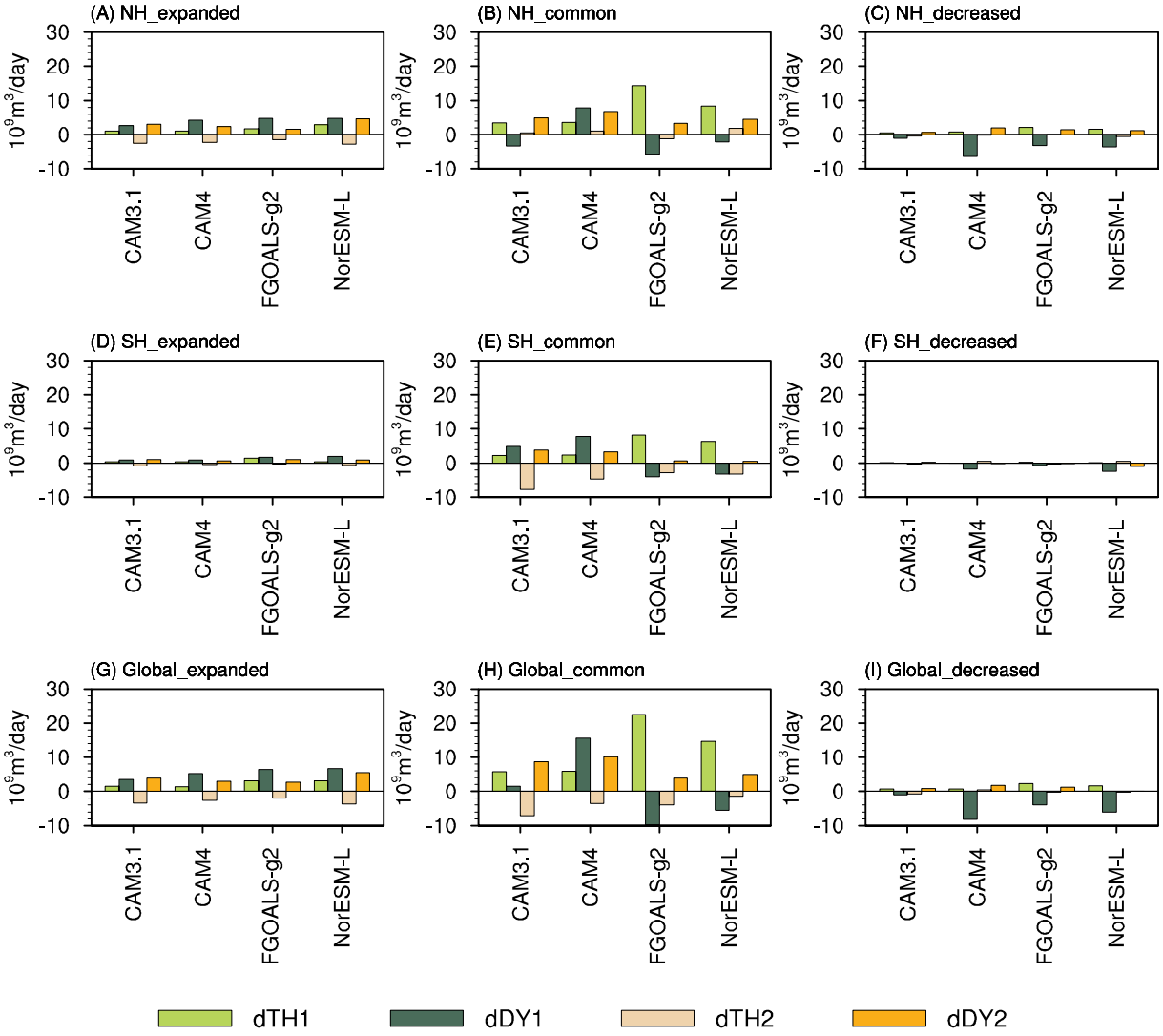

Fig. 8. Same as Fig. 7, but for thermodynamic and dynamic components of vertical moisture advection (indicated by yellow green and dark green bars, respectively) and horizontal moisture advection (indicated by light ivory and orange bars). The moisture budget method for thermodynamic and dynamic components is shown in supplementary Formula 4. (For interpretation of the references to colour in this figure legend, the reader is referred to the web version of this article.)

relative to the present state (Molnar, 2008), and such a picture implicates a wildly drier condition and agrees with the simulated monsoon precipitation decrease in those regions. Taken together, the simulated monsoon precipitation variations in northern Africa, Asia, northern Australia, Central America, and eastern South America are roughly in accord with geological evidence.

4.2. Implications for the Pliocene carbon cycle

Since the late Pliocene, the sustained major Northern Hemisphere continental glaciations developed (Raymo, 1994; Maslin et al., 1998), and the global climate evolved into the present bipolar glaciated state with the glacial–interglacial cycle. This transition is proposed to relate to the orbital configuration and the decrease in atmospheric CO_2 (Maslin et al., 1998; Lunt et al., 2008). The atmospheric CO_2 concentration during the Pliocene was about 50–120 ppm higher compared to the pre-industrial (280 ppm), and decreased relatively rapidly between 3.2 and 2.8 Ma (Seki et al., 2010). The decrease in atmospheric CO_2 during the late Pliocene is proposed to act as the main controlling factor to the development of Greenland glaciation (Lunt et al., 2008). Then the underlying mechanism of how the atmospheric CO_2 decreased during the late Pliocene is the key to those hypotheses. One possible explanation attributes the decrease in atmospheric CO_2 to the intensified Asian monsoon from 3.5 to 2.7 Ma (Zhang et al., 2009; Wan et al., 2012).

To what extent the locally reconstructed monsoon variation using scattered geological evidence can represent the overall Asian monsoon change is still questioned. In this study, multi-model ensemble mean shows that the Asian land monsoon intensifies (increases by 14.0% for Asian land monsoon precipitation and by 3.1% for its intensity) during the mid-Piacenzian. Such quantifications clearly indicate that the wetter condition during the pre-Quaternary period covers a large extent of Asian monsoon-dominated regions.

The intensified Asian monsoon can contribute to the decrease of atmospheric CO_2 on geological scale through the following ways. First, warmer and wetter conditions in major Asian monsoon-dominated regions would enhance silicate chemical weathering rate (White and Blum, 1995), which acts as a large sink of atmospheric CO_2 over geological timescales (Walker et al., 1981; Berner et al., 1983). Second, the stronger monsoon would boost biologic production and further increase the amount of organic carbon burial in marine sediments through riverine transport. Third, the stronger monsoon would increase runoff and accelerate the continental erosion rate, especially in the Himalaya and southern Tibetan Plateau regions, where the monsoon precipitation increases largely (Fig. 3); and the accelerated continental erosion rate can not only promote further the

Table 2
Geological evidence used to reconstruct the mid-Piacenzian environment.

Site	Location	Proxy data	Age (Ma BP)	Geological evidence compared to recent or late Quaternary climate	Reconstructed environment	Reference
***First Group* (direct evidence)**						
Qinghai Lake, Northeastern Tibetan Plateau	36°39′42.7″N, 100°23′23.7″E	Sediment lithology and clay minerals	Mid-Piacenzian	Deeper lake-level hinted by sediment lithology and mean grain size; higher ratio of kaolinite/(illite + chlorite), higher ratio of chlorite/illite	Wetter	Fu et al. (2013); Zeng et al. (2014)
Western Qaidam Basin (SG-1), Northeastern Tibetan Plateau	38°24′35.3″N, 92°30′32.7″E	Sediment lithology	2.8–2.5	Relatively larger and deeper lake-level (sedimentary textures and structures demonstrate a trend of lake shrinkage since the late Pliocene)	Wetter	Wang et al. (2012b)
		Geochemical proxies	2.8–2.5	Higher calcium-bound phosphorus, higher Total Organic Carbon (TOC, a biologic production proxy), more paleolake nutrient supply in the drainage	Wetter	Yang et al. (2013)
Western Qaidam Basin (SG-3), Northeastern Tibetan Plateau	38°22′47.8″N, 91°44′53.43″E	Pollen	3.1–2.6	Higher ratios of Artemisia to Chenopodiaceae, lower ratio of Non Arboreal Pollen to Arboreal Pollen, lower percentage of xerophytic, higher percentage of conifer, ecological environment was steppe compared with desert in late quaternary, more moisture over the region	Wetter	Cai et al. (2012); Miao et al. (2013)
Chaona, Chinese Loess Plateau	35°7′N, 107°12′E	Pollen	3.0–2.6	Lower ln (Non Arboreal Pollen to Arboreal Pollen) values, higher percentage of conifer, ecological environment was cupressaceae forest vegetation compared with steppe vegetation in late quaternary	Wetter	Wu et al. (2007)
		Magnetic parameters	3.3–2.6	Based on χ_{ARM}/SIRM variation, quantitatively reconstruct annual precipitation in the region		Nie et al. (2014)
Lingtai, Chinese Loess Plateau	35°00′33″N, 107°30′33″E	Pedogenesis indices	Mid-Piacenzian	Higher ratio of free to total Fe_2O_3, and higher soil weathering intensity	Wetter	Ding et al. (2001); Yang and Ding (2001)
	35°4′N, 107°33′E	Geochemical proxy	Pre-Quaternary	Higher ratio of $^{87}Sr/^{86}Sr$ of calcites, and stronger chemical weathering	Wetter	Rao et al. (2008)
Jingbian, Chinese Loess Plateau	37°40′54″N, 108°31′15″E	desert margin index	Mid-Piacenzian	Less sand-sized particle content of loess within loess near desert margin, hinting Mu Us Desert margin lied more northwardly	Wetter	Ding et al. (1995); Ding et al. (2005)
Baishui, Chinese Loess Plateau	35°24′10″N, 106°56′43″E	Geochemical proxy	Mid-Piacenzian	Higher chemical index of alteration value	Wetter	Xiong et al. (2010)
Eryuan, West Yunnan	26°00′N, 99°49′E	Pollen	Pliocene	Based on coexistence approach on palynological data, precipitation slightly decreased with a mid-value of $-26.8\,mm\,yr^{-1}$ (between -459–$405.4\,mm\,yr^{-1}$)	Slightly drier	Kou et al. (2006)
Yangyi, West Yunnan	24°57′ N, 99°15′ E	Pollen	Pliocene	Based on coexistence approach on palynological data, precipitation slightly increased with a mid-value of $59.7\,mm\,yr^{-1}$ (between -168.9–$288.3\,mm\,yr^{-1}$)	Slightly wetter	Kou et al. (2006)
Longling, West Yunnan	24°41′N, 98°50′E	Pollen	Pliocene	Based on coexistence approach on palynological data, precipitation extremely varied by -1306.2–$-867.3\,mm\,yr^{-1}$, with a mid-value of $-786.75\,mm\,yr^{-1}$	Drier	Kou et al. (2006)
Turkana Basin, northern Africa	~3.8°N, ~36.6°E	paleobotany	Mid-Piacenzian	Less soil carbonate $\delta^{13}C$, and smaller proportion of C_4 biomass	Wetter	Cerling (1992); Wynn (2004)
San Pedro La Cocona, southeastern Guatemala, North America	15°45′N, 88°42′W	Paleobotany	Pliocene	Tropical rain forest was absent or poorly represented	Drier	Graham (1998)
Zent, southeastern Costa Rica, North America	10°02′N, 83°17′W	Paleobotany	Pliocene	Annual precipitation is estimated at near the present level	Not significantly changed	Graham (1998); Graham and Dilcher (1998)
***Second group* (*indirect evidence*)**						
ODP 885/886	885 (44°41.298′ N, 168°16.320′ W) 886 (44°41.382′ N, 168°14.400′ W)	Eolian dust	Mid-Piacenzian	Less mass accumulation rates of terrigenous (eolian) dust	Asian inland was wetter	Rea et al. (1998)
DSDP 231	11°53.4120′N, 48°14.7120′E	Paleobotany	3.4–3.2	Less plant wax biomarkers $\delta^{13}C$, less C_4 plants component of the landscape	Northeast Africa was wetter	Feakins et al. (2005)
		Eolian dust	Mid-Piacenzian	Less mass accumulation rates of terrigenous (eolian) dust	Northeast Africa was wetter	deMenocal (1995)
ODP 659	18°4.632′N, 21°1.572′W	Eolian dust	Mid-Piacenzian	Less mass accumulation rates of terrigenous (eolian) dust	West Africa was wetter	deMenocal (1995)
ODP 662/663	662 (1°23.412′ S, 11°44.352′ W) 663 (1°11.868′ S, 11°52.710′ W)	Eolian dust	Mid-Piacenzian	Less mass accumulation rates of terrigenous (eolian) dust	West Africa was wetter	deMenocal (1995)

(*continued on next page*)

Table 2 (*continued*)

Site	Location	Proxy data	Age (Ma BP)	Geological evidence compared to recent or late Quaternary climate	Reconstructed environment	Reference
ODP 664	0°6.438′N, 23°13.650′W	Eolian dust	Mid-Piacenzian	Less mass accumulation rates of terrigenous (eolian) dust	West Africa was wetter	deMenocal (1995)
ODP 721/722	721 (16°40.668′ N, 59°51.870′ E) 722 (16°37.308′ N, 59°47.718′ E)	Eolian dust	Mid-Piacenzian	Less mass accumulation rates of terrigenous (eolian) dust	Northeast Africa was wetter	deMenocal (1995)

silicate weathering reaction through the exposure of fresh silicate in the critical zone (Raymo et al., 1988; Raymo and Ruddiman, 1992), but also reduce organic carbon oxidation loess during transport and thus give rise to more organic carbon in the marginal sea (Galy et al., 2007, 2015). In total, such a warmer and wetter environment would lead to the increase in continental silicate weathering flux and terrestrial organic carbon burial flux in the marginal seas, which forms the major, even dominant, atmospheric CO_2 sink over geological timescales (Raymo and Ruddiman, 1992; France-Lanord and Derry, 1997; Raymo et al., 1988; Galy et al., 2007, 2015). Evidently, the estimated silicate weathering rate all over the entire Asia indicates higher chemical weathering intensity in the mid-late Pliocene than in the Quaternary (Wan et al., 2012, their Fig. 2) and suggests a plausible link to atmospheric CO_2 since the late-Pliocene. Also, as it has been stated, the organic carbon burial was large in the Pliocene and generally reduced afterwards (Raymo, 1997). The enhanced CO_2 consumption induced by the intensified Asian monsoon could be an explanation to the atmospheric CO_2 decrease during the late Pliocene.

Further, the mid-Piacenzian increased GLMP (5.8% or $14.7 \times 10^9\ m^3\ day^{-1}$) comes mainly from not only Asia (increase by 14.0%) but also northern Africa (increase by 20.0%) and northern Australia (increase by 56.0%). The intensified monsoon in northern Africa and northern Australia could also contribute to the atmospheric CO_2 drop in similar ways. Therefore, generally intensified global land monsoon during the Pliocene possibly account for the subsequent atmospheric CO_2 drop.

4.3. Uncertainties

In this paper, we provide only the simulated changes in the mid-Piacenzian land monsoon and its possible linkage to the atmospheric CO_2 drawdown afterward but no quantitative estimation of direct CO_2 consumption amount by silicate weathering and organic carbon burial in Asian monsoon region or in the world. Besides, other carbon cycle processes are not considered at the moment, such as carbon source from volcanic emissions and the weathering of basaltic rock (Li and Elderfield, 2013; Molnar and Cronin, 2015) in a warmer world. As such, it is difficult to directly evaluate the role of intensified mid-Piacenzian land monsoon on the atmospheric CO_2 drawdown in the late Pliocene. Also, both rock uplift and stronger monsoon precipitation could enhance the physical denudation and associated silicate weathering rates in the Himalaya and Tibetan Plateau in the Pliocene (e.g., Wan et al., 2012). The tectonic factor is another possible candidate for the atmospheric CO_2 drawdown in the late Pliocene, although it is still under debate (e.g., Zheng et al., 2014).

On the whole, both simulations and geological evidence are compatible with the hypothesis that on geological timescales, the intensified mid-Piacenzian Asian monsoon could enhance rock weathering and/or accelerate organic carbon burial and contribute to the lowering of atmospheric CO_2 concentration and the subsequent onset of the sustained major Northern Hemisphere glaciation (Lunt et al., 2008; Zhang et al., 2009; Wan et al., 2012). The region of intensified monsoon emphasized in such a hypothesis could further extend from Asia to the globe in general. To get an in-depth understanding or a persuasive test of that hypothesis, a quantitative estimation of the amount of atmospheric CO_2 consumptions induced by intensified monsoon during the Pliocene requires to be explored.

5. Conclusions

In this study, model simulations show that the mid-Piacenzian GLMA and GLMP increase relative to the pre-industrial period by an average of 7.3% and 5.8%, respectively, and that GLMPI varies slightly (by −1.4%). It is the variation of GLMA, rather than of GLMPI, that mainly accounts for the GLMP change. The underlying mechanisms are related to the modification of anomalous inland water vapor transportation due to the weakening of large-scale meridional thermal contrast. Based on the analysis of moisture budget, the increased vertical moisture advection and evaporation are mainly responsible for the global land monsoon change. The simulated monsoon precipitation variations are roughly consistent with the

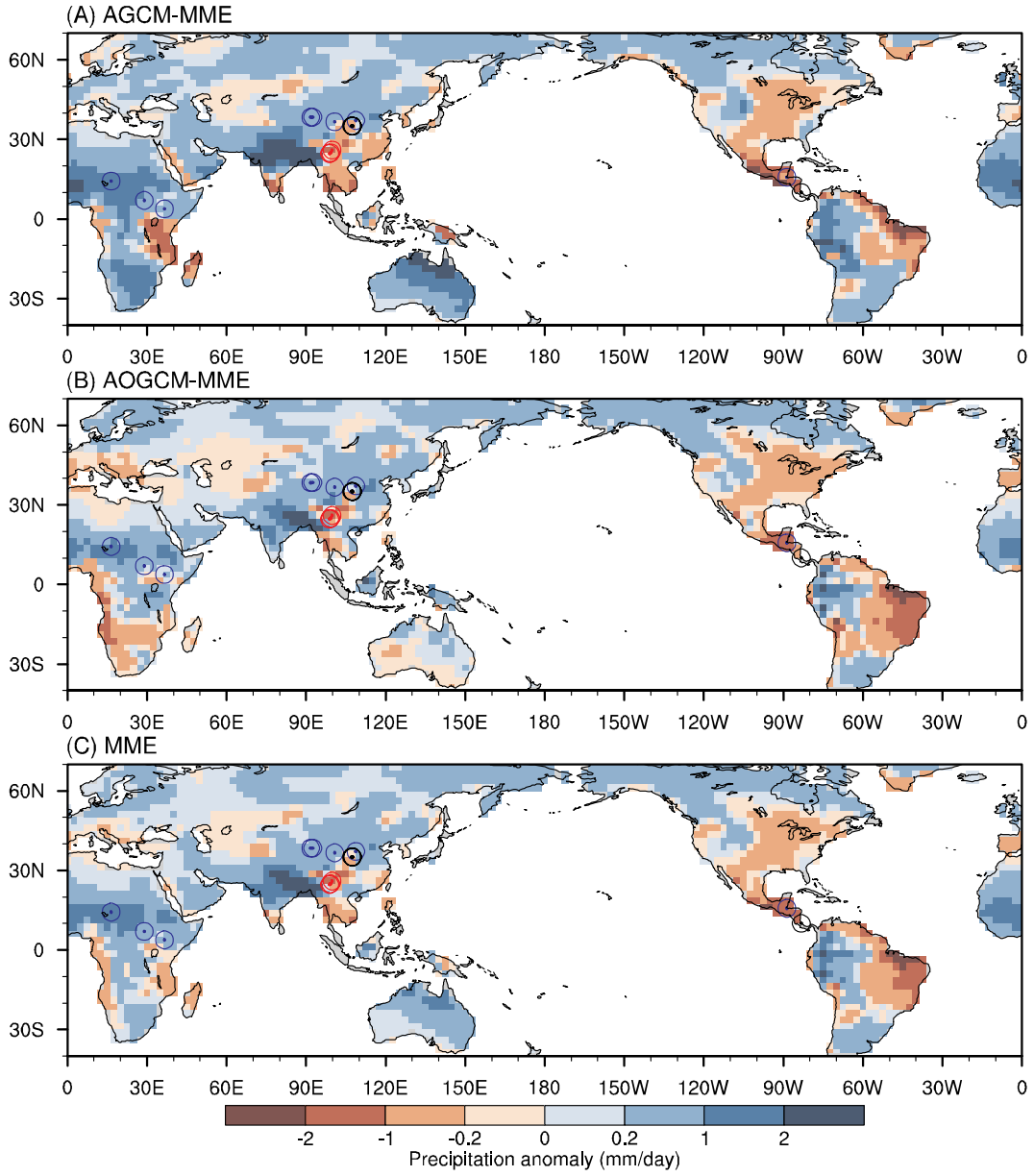

Fig. 9. Anomaly of summer precipitation in the mid-Piacenzian relative to the pre-industrial period from the ensemble mean of (A) AGCMs, (B) AOGCMs, and (C) all 14 models. In panels (A) to (C), the summer precipitation stands for May–September (November–March) precipitation in the northern (southern) hemisphere (shading, units: mm day^{-1}). Circles with dot show mid-Piacenzian paleoenvironment in land monsoon domains reconstructed by the first type of geological evidence listed in Table 2 (blue, green, and red markers stand for wetter, normal, and drier environments, respectively). (For interpretation of the references to colour in this figure legend, the reader is referred to the web version of this article.)

reconstructed geological evidence in northern Africa, Asia, northern Australia, Central America, and eastern South America.

Moreover, the increased GLMP is mainly derived from northern Africa, Asia, and northern Australia. Together with geological evidence and an overall quite high denudation rates in these regions (Walling and Webb, 1983), model simulations support the hypothesis that the intensified mid-Piacenzian Asian monsoon or generally intensified land monsoon on a global scale contributes to the lowering of atmospheric CO_2 concentration and the subsequent onset of the sustained major Northern Hemisphere glaciations. In the future, the hypothesis still needs to be tested by quantitative estimation of CO_2 consumption amount by silicate weathering and organic carbon burial in Asian or global monsoon region during the late Pliocene.

Acknowledgments

We sincerely acknowledge the Pliocene Model Intercomparison Project phase 1 (PlioMIP1) modeling groups (listed in Table 1 of this paper) for producing and sharing their model output. Grateful acknowledgements are given to Drs. Zhongshi Zhang, Qing Yan, and W.-L. Chan for providing model data, and to the anonymous reviewers for their constructive comments. This work is supported by the Strategic Priority Research Program of the Chinese Academy of Sciences (Grant no. XDA20070103), the National Natural Science Foundation of China (Grant nos. 41421004 and 41625018), and the China Postdoctoral Science Foundation funded project (Grant no. 2015M581154).

Appendix A. Supplementary data

Supplementary data to this article can be found online at https://doi.org/10.1016/j.palaeo.2018.06.027.

References

Adler, R.F., Huffman, G.J., Chang, A., Ferraro, R., Xie, P.-P., Janowiak, J., Rudolf, B., Schneider, U., Curtis, S., Bolvin, D., Gruber, A., Susskind, J., Arkin, P., Nelkin, E., 2003. The version-2 Global Precipitation Climatology Project (GPCP) monthly precipitation analysis (1979–present). J. Hydrometeorol. 4, 1147–1167.

An, Z., Kutzbach, J.E., Prell, W.L., Porter, S.C., 2001. Evolution of Asian monsoons and phased uplift of the Himalaya–Tibetan plateau since Late Miocene times. Nature 411, 62–66.

An, Z., Wu, G., Li, J., Sun, Y., Liu, Y., Zhou, W., Cai, Y., Duan, A., Li, L., Mao, J., Cheng, H., Shi, Z., Tan, L., Yan, H., Ao, H., Chang, H., Feng, J., 2015. Global monsoon dynamics and climate change. Annu. Rev. Earth Planet. Sci. 43, 29–77.

Ao, H., Roberts, A.P., Dekkers, M.J., et al., 2016. Late Miocene–Pliocene Asian monsoon intensification linked to Antarctic ice-sheet growth. Earth Planet. Sci. Lett. 444, 75–87.

Berner, R.A., Lasaga, A.C., Garrels, R.M., 1983. The carbonate-silicate geochemical cycle and its effect on atmospheric carbon dioxide over the past 100 million years. Am. J. Sci. 283, 641–683.

Bragg, F.J., Lunt, D.J., Haywood, A.M., 2012. Mid-Pliocene climate modelled using the UK Hadley Centre Model: PlioMIP experiments 1 and 2. Geosci. Model Dev. 5, 1109–1125.

Cai, M., Fang, X., Wu, F., Miao, Y., Appel, E., 2012. Pliocene–Pleistocene stepwise drying of Central Asia: evidence from paleomagnetism and sporopollen record of the deep borehole SG-3 in the western Qaidam Basin, NE Tibetan Plateau. Glob. Planet. Chang. 94–95, 72–81.

Cerling, T.E., 1992. Development of grasslands and savannas in East Africa during the Neogene. Palaeogeogr. Palaeoclimatol. Palaeoecol. 97, 241–247.

Chan, W.-L., Abe-Ouchi, A., Ohgaito, R., 2011. Simulating the mid-Pliocene climate with the MIROC general circulation model: experimental design and initial results. Geosci. Model Dev. 4, 1035–1049.

Chandler, M., Rind, D., Thompson, R., 1994. Joint investigations of the middle Pliocene climate II: GISS GCM northern hemisphere results. Glob. Planet. Chang. 9, 197–219.

Chandler, M.A., Sohl, L.E., Jonas, J.A., Dowsett, H.J., Kelley, M., 2013. Simulations of the mid-Pliocene warm period using two versions of the NASA/GISS ModelE2-R coupled model. Geosci. Model Dev. 6, 517–531.

Cheng, H., Sinha, A., Wang, X., Cruz, F.W., Edwards, R.L., 2012. The global paleomonsoon as seen through speleothem records from Asia and the Americas. Clim. Dyn. 39, 1045–1062.

Chou, C., Lan, C.W., 2012. Changes in the annual range of precipitation under global warming. J. Clim. 25, 222–235.

Chou, C., Chiang, J.C., Lan, C.W., Chung, C.H., Liao, Y.C., Lee, C.J., 2013. Increase in the range between wet and dry season precipitation. Nat. Geosci. 6, 263–267.

Clemens, S.C., Prell, W.L., 1990. Late Pleistocene variability of Arabian Sea summer monsoon winds and continental aridity: eolian records from the lithogenic component of deep-sea sediments. Paleoceanography 5, 109–145.

Clemens, S.C., Murray, D.W., Prell, W.L., 1996. Nonstationary phase of the Plio-Pleistocene Asian monsoon. Science 274, 943–948.

Contoux, C., Ramstein, G., Jost, A., 2012. Modelling the mid-Pliocene warm period climate with the IPSL coupled model and its atmospheric component LMDZ5A. Geosci. Model Dev. 5, 903–917.

Contoux, C., Jost, A., Ramstein, G., Sepulchre, P., Krinner, G., Schuster, M., 2013. Megalake Chad impact on climate and vegetation during the late Pliocene and the mid-Holocene. Clim. Past 9, 1417–1430.

Corvec, S., Fletcher, C.G., 2017. Changes to the tropical circulation in the mid-Pliocene and their implications for future climate. Clim. Past 13, 135–147.

Cronin, T.M., Whatley, R., Wood, A., Tsukagoshi, A., Ikeya, N., Brouwers, E.M., Briggs, W.M., 1993. Microfaunal evidence for elevated Pliocene temperatures in the Arctic Ocean. Paleoceanography 8, 161–173.

Dai, A., Li, H., Sun, Y., Hong, L.-C., LinHo, Chou, C., Zhou, T., 2013. The relative roles of upper and lower tropospheric thermal contrasts and tropical influences in driving Asian summer monsoons. J. Geophys. Res. Atmos. 118, 7024–7045.

Ding, Z., Liu, T., Rutter, N.W., Yu, Z., Guo, Z., Zhu, R., 1995. Ice-volume forcing of East Asian winter monsoon variations in the past 800,000 years. Quat. Res. 44, 149–159.

Ding, Z.L., Xiong, S.F., Sun, J.M., Yang, S.L., Gu, Z.Y., Liu, T.S., 1999. Pedostratigraphy and paleomagnetism of a ~7.0 Ma eolian loess–red clay sequence at Lingtai, Loess Plateau, north-central China and the implications for paleomonsoon evolution. Palaeogeogr. Palaeoclimatol. Palaeoecol. 152, 49–66.

Ding, Z.L., Yang, S.L., Sun, J.M., Liu, T.S., 2001. Iron geochemistry of loess and red clay deposits in the Chinese Loess Plateau and implications for long-term Asian monsoon evolution in the last 7.0 Ma. Earth Planet. Sci. Lett. 185, 99–109.

Ding, Z.L., Derbyshire, E., Yang, S.L., Sun, J.M., Liu, T.S., 2005. Stepwise expansion of desert environment across northern China in the past 3.5 Ma and implications for monsoon evolution. Earth Planet. Sci. Lett. 237, 45–55.

Dowsett, H., 2007. Faunal re-evaluation of mid-Pliocene conditions in the western equatorial Pacific. Micropaleontology 53, 447–456.

Dowsett, H.J., Robinson, M.M., 2009. Mid-Pliocene equatorial Pacific sea surface temperature reconstruction: a multi-proxy perspective. Philos. Trans. R. Soc. A Math. Phy. Eng. Sci. 367, 109–125.

Dowsett, H.J., Robinson, M.M., Foley, K.M., 2009. Pliocene three-dimensional global ocean temperature reconstruction. Clim. Past 5, 769–783.

Dowsett, H., Robinson, M., Haywood, A., Salzmann, U., Hill, D., Sohl, L., Chandler, M., Williams, M., Foley, K., Stoll, D., 2010. The PRISM3D paleoenvironmental reconstruction. Stratigraphy 7, 123–139.

Feakins, S.J., deMenocal, P.B., Eglinton, T.I., 2005. Biomarker records of late Neogene changes in northeast African vegetation. Geology 33, 977–980.

France-Lanord, C., Derry, L.A., 1997. Organic carbon burial forcing of the carbon cycle from Himalayan erosion. Nature 390, 65–67.

Fu, C., An, Z., Qiang, X., Bloemendal, J., Song, Y., Chang, H., 2013. Magnetostratigraphic determination of the age of ancient Lake Qinghai, and record of the East Asian monsoon since 4.63 Ma. Geology 41, 875–878.

Galy, V., France-Lanord, C., Beyssac, O., Faure, P., Kudrass, H., Palhol, F., 2007. Efficient organic carbon burial in the Bengal fan sustained by the Himalayan erosional system. Nature 450, 407–410.

Galy, V., Peucker-Ehrenbrink, B., Eglinton, T., 2015. Global carbon export from the terrestrial biosphere controlled by erosion. Nature 521, 204–207.

Graham, A., 1998. Studies in Neotropical paleobotany. XI. Late Tertiary vegetation and environments of southeastern Guatemala: palynofloras from the Mio-Pliocene Padre Miguel Group and the Pliocene Herrería Formation. Am. J. Bot. 85, 1409–1425.

Graham, A., Dilcher, D.L., 1998. Studies in Neotropical paleobotany. XII. A palynoflora from the Pliocene Rio Banano Formation of Costa Rica and the Neogene vegetation of Mesoamerica. Am. J. Bot. 85, 1426–1438.

Guo, Z.T., Ruddiman, W.F., Hao, Q.Z., Wu, H.B., Qiao, Y.S., Zhu, R.X., Peng, S.Z., Wei, J.J., Yuan, B.Y., Liu, T.S., 2002. Onset of Asian desertification by 22 Myr ago inferred from loess deposits in China. Nature 416, 159–163.

Harrison, S.P., Bartlein, P.J., Prentice, I.C., 2016. What have we learnt from palaeoclimate simulations? J. Quat. Sci. 31, 363–385.

Haywood, A.M., Dowsett, H.J., Otto-Bliesner, B., Chandler, M.A., Dolan, A.M., Hill, D.J., Lunt, D.J., Robinson, M.M., Rosenbloom, N., Salzmann, U., Sohl, L.E., 2010. Pliocene Model Intercomparison Project (PlioMIP): experimental design and boundary conditions (experiment 1). Geosci. Model Dev. 3, 227–242.

Haywood, A.M., Dowsett, H.J., Robinson, M.M., Stoll, D.K., Dolan, A.M., Lunt, D.J., Otto-Bliesner, B., Chandler, M.A., 2011. Pliocene Model Intercomparison Project (PlioMIP): experimental design and boundary conditions (experiment 2). Geosci. Model Dev. 4, 571–577.

Haywood, A.M., Hill, D.J., Dolan, A.M., Otto-Bliesner, B.L., Bragg, F., Chan, W.L., Chandler, M.A., Contoux, C., Dowsett, H.J., Jost, A., Kamae, Y., Lohmann, G., Lunt, D.J., Abe-Ouchi, A., Pickering, S.J., Ramstein, G., Rosenbloom, N.A., Salzmann, U., Sohl, L., Stepanek, C., Ueda, H., Yan, Q., Zhang, Z., 2013. Large-scale features of Pliocene climate: results from the Pliocene Model Intercomparison Project. Clim. Past 9, 191–209.

Haywood, A.M., Dowsett, H.J., Dolan, A.M., 2016. Integrating geological archives and climate models for the mid-Pliocene warm period. Nat. Commun. 7, 10646. https://doi.org/10.1038/ncomms10646.

Hsu, P.-c., Li, T., Luo, J.-J., Murakami, H., Kitoh, A., Zhao, M., 2012. Increase of global monsoon area and precipitation under global warming: a robust signal? Geophys. Res. Lett. 39, L06701. https://doi.org/10.1029/2012GL051037.

Huffman, G.J., Adler, R.F., Bolvin, D.T., Gu, G., 2009. Improving the global precipitation record: GPCP version 2.1. Geophys. Res. Lett. 36, L17808. https://doi.org/10.1029/2009GL040000.

Jiang, D., Wang, H., Ding, Z., Lang, X., Drange, H., 2005. Modeling the middle Pliocene climate with a global atmospheric general circulation model. J. Geophys. Res. 110, D14107. https://doi.org/10.1029/2004JD005639.

Jiang, D., Tian, Z., Lang, X., 2015a. Mid-Holocene global monsoon area and precipitation from PMIP simulations. Clim. Dyn. 44, 2493–2512.

Jiang, D., Tian, Z., Lang, X., Kageyama, M., Ramstein, G., 2015b. The concept of global monsoon applied to the last glacial maximum: a multi-model analysis. Quat. Sci. Rev. 126, 126–139.

Kou, X.-Y., Ferguson, D., Xu, J.-X., Wang, Y.-F., Li, C.-S., 2006. The reconstruction of paleovegetation and paleoclimate in the Late Pliocene of West Yunnan, China. Clim. Chang. 77, 431–448.

Lee, J.-Y., Wang, B., 2014. Future change of global monsoon in the CMIP5. Clim. Dyn. 42, 101–119.

Li, G., Elderfield, H., 2013. Evolution of carbon cycle over the past 100 million years. Geochim. Cosmochim. Acta 103, 11–25.

Li, C., Yanai, M., 1996. The onset and interannual variability of the Asian summer monsoon in relation to land–sea thermal contrast. J. Clim. 9, 358–375.

Liu, T.S., Ding, Z.L., 1998. Chinese loess and the paleomonsoon. Annu. Rev. Earth Planet. Sci. 26, 111–145.

Liu, J., Wang, B., Ding, Q., Kuang, X., Soon, W., Zorita, E., 2009. Centennial variations of the global monsoon precipitation in the last millennium: results from ECHO-G model. J. Clim. 22, 2356–2371.

Liu, J., Wang, B., Cane, M.A., Yim, S.-Y., Lee, J.-Y., 2013. Divergent global precipitation changes induced by natural versus anthropogenic forcing. Nature 493, 656–659.

Lunt, D.J., Foster, G.L., Haywood, A.M., Stone, E.J., 2008. Late Pliocene Greenland glaciation controlled by a decline in atmospheric CO_2 levels. Nature 454, 1102–1105.

Lunt, D.J., Haywood, A.M., Schmidt, G.A., Salzmann, U., Valdes, P.J., Dowsett, H.J., 2010. Earth system sensitivity inferred from Pliocene modelling and data. Nat. Geosci. 3, 60–64.

Lunt, D.J., Haywood, A.M., Schmidt, G.A., Salzmann, U., Valdes, P.J., Dowsett, H.J., Loptson, C.A., 2012. On the causes of mid-Pliocene warmth and polar amplification. Earth Planet. Sci. Lett. 321–322, 128–138.

Lunt, D.J., Elderfield, H., Pancost, R., Ridgwell, A., Foster, G.L., Haywood, A., Kiehl, J., Sagoo, N., Shields, C., Stone, E.J., Valdes, P., 2013. Warm climates of the past—a lesson for the future? Philos. Trans. R. Soc. A Math. Phys. Eng. Sci. 371, 20130146. https://doi.org/10.1098/rsta.2013.0146.

Martin, H.A., 2006. Cenozoic climatic change and the development of the arid vegetation in Australia. J. Arid Environ. 66, 533–563.
Maslin, M.A., Li, X.S., Loutre, M.F., Berger, A., 1998. The contribution of orbital forcing to the progressive intensification of Northern Hemisphere glaciation. Quat. Sci. Rev. 17, 411–426.
deMenocal, P.B., 1995. Plio-Pleistocene African climate. Science 270, 53–59.
Miao, Y.F., Fang, X.M., Wu, F.L., Cai, M.T., Song, C.H., Meng, Q.Q., Xu, L., 2013. Late Cenozoic continuous aridification in the western Qaidam Basin: evidence from sporopollen records. Clim. Past 9, 1863–1877.
Miller, K.G., Wright, J.D., Browning, J.V., Kulpecz, A., Kominz, M., Naish, T.R., Cramer, B.S., Rosenthal, Y., Peltier, W.R., Sosdian, S., 2012. High tide of the warm Pliocene: implications of global sea level for Antarctic deglaciation. Geology 40, 407–410.
Molnar, P., 2008. Closing of the Central American Seaway and the Ice Age: a critical review. Paleoceanography 23, PA2201. https://doi.org/10.1029/2007PA001574.
Molnar, P., Cronin, T.W., 2015. Growth of the maritime continent and its possible contribution to recurring Ice Ages. Paleoceanography 30, 196–225.
Nie, J., Stevens, T., Song, Y., et al., 2014. Pacific freshening drives Pliocene cooling and Asian monsoon intensification. Sci. Rep. 4, 5474. https://doi.org/10.1038/srep05474.
Otero, O., Pinton, A., Mackaye, H.T., Likius, A., Vignaud, P., Brunet, M., 2010. The Early/Late Pliocene ichthyofauna from Koro-Toro, Eastern Djurab, Chad. Geobios 43, 241–251.
Pound, M.J., Tindall, J., Pickering, S.J., Haywood, A.M., Dowsett, H.J., Salzmann, U., 2014. Late Pliocene lakes and soils: a global data set for the analysis of climate feedbacks in a warmer world. Clim. Past 10, 167–180.
Rao, W., Chen, J., Yang, J., Ji, J., Zhang, G., Chen, J., 2008. Strontium isotopic and elemental characteristics of calcites in the eolian dust profile of the Chinese Loess Plateau during the past 7 Ma. Geochem. J. 42, 493–506.
Raymo, M.E., 1994. The initiation of northern hemisphere glaciation. Annu. Rev. Earth Planet. Sci. 22, 353–383.
Raymo, M.E., 1997. Carbon cycle models: how strong are the constraints? In: Ruddiman, W.F. (Ed.), Tectonic Uplift and Climate Change. Springer US, pp. 367–381.
Raymo, M.E., Ruddiman, W.F., 1992. Tectonic forcing of late Cenozoic climate. Nature 359, 117–122.
Raymo, M.E., Ruddiman, W.F., Froelich, P.N., 1988. Influence of late Cenozoic mountain building on ocean geochemical cycles. Geology 16, 649–653.
Rea, D.K., 1994. The paleoclimatic record provided by eolian deposition in the deep sea: the geologic history of wind. Rev. Geophys. 32, 159–195.
Rea, D.K., Leinen, M., 1988. Asian aridity and the zonal westerlies: Late Pleistocene and Holocene record of eolian deposition in the northwest Pacific Ocean. Palaeogeogr. Palaeoclimatol. Palaeoecol. 66, 1–8.
Rea, D.K., Snoeckx, H., Joseph, L.H., 1998. Late Cenozoic eolian deposition in the North Pacific: Asian drying, Tibetan uplift, and cooling of the northern hemisphere. Paleoceanography 13, 215–224.
Robinson, M.M., 2009. New quantitative evidence of extreme warmth in the Pliocene Arctic. Stratigraphy 6, 265–275.
Robinson, M.M., Dowsett, H.J., Dwyer, G.S., Lawrence, K.T., 2008. Reevaluation of mid-Pliocene North Atlantic Sea surface temperatures. Paleoceanography 23, PA3213. https://doi.org/10.1029/2008PA001608.
Rosenbloom, N.A., Otto-Bliesner, B.L., Brady, E.C., Lawrence, P.J., 2013. Simulating the mid-Pliocene warm period with the CCSM4 model. Geosci. Model Dev. 6, 549–561.
Salzmann, U., Haywood, A.M., Lunt, D.J., Valdes, P.J., Hill, D.J., 2008. A new global biome reconstruction and data-model comparison for the Middle Pliocene. Glob. Ecol. Biogeogr. 17, 432–447.
Salzmann, U., Haywood, A.M., Lunt, D.J., 2009. The past is a guide to the future? Comparing middle Pliocene vegetation with predicted biome distributions for the twenty-first century. Philos. Trans. R. Soc. A Math. Phy. Eng. Sci. 367, 189–204.
Schmidt, G.A., 2010. Enhancing the relevance of palaeoclimate model/data comparisons for assessments of future climate change. J. Quat. Sci. 25, 79–87.
Schmidt, G.A., Annan, J.D., Bartlein, P.J., Cook, B.I., Guilyardi, E., Hargreaves, J.C., Harrison, S.P., Kageyama, M., LeGrande, A.N., Konecky, B., Lovejoy, S., Mann, M.E., Masson-Delmotte, V., Risi, C., Thompson, D., Timmermann, A., Tremblay, L.B., Yiou, P., 2014. Using palaeo-climate comparisons to constrain future projections in CMIP5. Clim. Past 10, 221–250.
Schuster, M., Duringer, P., Ghienne, J.-F., Roquin, C., Sepulchre, P., Moussa, A., Lebatard, A.-E., Mackaye, H.T., Likius, A., Vignaud, P., Brunet, M., 2009. Chad Basin: Paleoenvironments of the Sahara since the Late Miocene. Compt. Rendus Geosci. 341, 603–611.
Seki, O., Foster, G.L., Schmidt, D.N., Mackensen, A., Kawamura, K., Pancost, R.D., 2010. Alkenone and boron-based Pliocene pCO_2 records. Earth Planet. Sci. Lett. 292, 201–211.
Sloan, L.C., Crowley, T.J., Pollard, D., 1996. Modeling of middle Pliocene climate with the NCAR GENESIS general circulation model. Mar. Micropaleontol. 27, 51–61.
Sohl, L.E., Chandler, M.A., Schmunk, R.B., Mankoff, Ken, Jonas, J.A., Foley, K.M., Dowsett, H.J., 2009. PRISM3/GISS Topographic Reconstruction: U.S. Geological Survey Data Series. 419 (6p).
Stepanek, C., Lohmann, G., 2012. Modelling mid-Pliocene climate with COSMOS. Geosci. Model Dev. 5, 1221–1243.
Sun, Y., An, Z., 2005. Late Pliocene-Pleistocene changes in mass accumulation rates of eolian deposits on the central Chinese Loess Plateau. J. Geophys. Res. 110, D23101. https://doi.org/10.1029/2005JD006064.
Sun, Y., An, Z., Clemens, S.C., Bloemendal, J., Vandenberghe, J., 2010. Seven million years of wind and precipitation variability on the Chinese Loess Plateau. Earth Planet. Sci. Lett. 297, 525–535.
Sun, Y., Zhou, T., Ramstein, G., Contoux, C., Zhang, Z., 2016. Drivers and mechanisms for enhanced summer monsoon precipitation over East Asia during the mid-Pliocene in the IPSL-CM5A. Clim. Dyn. 46, 1437–1457.
Thompson, R.S., Fleming, R.F., 1996. Middle Pliocene vegetation: reconstructions, paleoclimatic inferences, and boundary conditions for climate modeling. Mar. Micropaleontol. 27, 27–49.
Tiedemann, R., Sarnthein, M., Shackleton, N.J., 1994. Astronomic timescale for the Pliocene Atlantic $\delta^{18}O$ and dust flux records of Ocean Drilling Program Site 659. Paleoceanography 9, 619–638.
Trenberth, K.E., Stepaniak, D.P., Caron, J.M., 2000. The global monsoon as seen through the divergent atmospheric circulation. J. Clim. 13, 3969–3993.
Ueda, H., Iwai, A., Kuwako, K., Hori, M.E., 2006. Impact of anthropogenic forcing on the Asian summer monsoon as simulated by eight GCMs. Geophys. Res. Lett. 33, L06703. https://doi.org/10.1029/2005GL025336.
Vallé, F., Dupont, L.M., Leroy, S.A.G., Schefuß, E., Wefer, G., 2014. Pliocene environmental change in West Africa and the onset of strong NE trade winds (ODP Sites 659 and 658). Palaeogeogr. Palaeoclimatol. Palaeoecol. 414, 403–414.
Walker, J.C.G., Hays, P.B., Kasting, J.F., 1981. A negative feedback mechanism for the long-term stabilization of Earth's surface temperature. J. Geophys. Res. 86 (C10), 9776–9782.
Walling, D.E., Webb, B.W., 1983. Patterns of sediment yield. In: Gregory, K.J. (Ed.), Background to Palaeohydrology. Wiley, Chichester, UK, pp. 69–100.
Wan, S., Clift, P.D., Li, A., Yu, Z., Li, T., Hu, D., 2012. Tectonic and climatic controls on long-term silicate weathering in Asia since 5 Ma. Geophys. Res. Lett. 39, L15611. https://doi.org/10.1029/2012GL052377.
Wang, P., 2009. Global monsoon in a geological perspective. Chin. Sci. Bull. 54, 1113–1136.
Wang, B., Ding, Q., 2008. Global monsoon: dominant mode of annual variation in the tropics. Dyn. Atmos. Oceans 44, 165–183.
Wang, B., Liu, J., Kim, H.-J., Webster, P., Yim, S.-Y., 2012a. Recent change of the global monsoon precipitation (1979–2008). Clim. Dyn. 39, 1123–1135.
Wang, J., Fang, X., Appel, E., Song, C., 2012b. Pliocene–Pleistocene climate change at the NE Tibetan Plateau deduced from lithofacies variation in the drill core SG-1, western Qaidam Basin, China. J. Sediment. Res. 82, 933–952.
Wang, P.X., Wang, B., Cheng, H., Fasullo, J., Guo, Z.T., Kiefer, T., Liu, Z.Y., 2014. The global monsoon across timescales: coherent variability of regional monsoons. Clim. Past 10, 2007–2052.
Wang, P.X., Wang, B., Cheng, H., Fasullo, J., Guo, Z.T., Kiefer, T., Liu, Z.Y., 2017. The global monsoon across time scales: mechanisms and outstanding issues. Earth-Sci. Rev. 174, 84–121.
Webster, P.J., 1987. The elementary monsoon. In: Fein, J.S., Stephens, P.L. (Eds.), Monsoons. John Wiley, New York, pp. 3–32.
Webster, P.J., Magaña, V.O., Palmer, T.N., Shukla, J., Tomas, R.A., Yanai, M., Yasunari, T., 1998. Monsoons: processes, predictability, and the prospects for prediction. J. Geophys. Res. 103 (C7), 14451–14510.
White, A.F., Blum, A.E., 1995. Effects of climate on chemical weathering in watersheds. Geochim. Cosmochim. Acta 59, 1729–1747.
Wu, F., Fang, X., Ma, Y., Herrmann, M., Mosbrugger, V., An, Z., Miao, Y., 2007. Plio–quaternary stepwise drying of Asia: evidence from a 3-Ma pollen record from the Chinese Loess Plateau. Earth Planet. Sci. Lett. 257, 160–169.
Wynn, J.G., 2004. Influence of Plio-Pleistocene aridification on human evolution: evidence from paleosols of the Turkana Basin, Kenya. Am. J. Phys. Anthropol. 123, 106–118.
Xie, P., Arkin, P.A., 1997. Global precipitation: a 17-year monthly analysis based on gauge observations, satellite estimates, and numerical model outputs. Bull. Am. Meteorol. Soc. 78, 2539–2558.
Xiong, S., Ding, Z., Zhu, Y., Zhou, R., Lu, H., 2010. A ~6 Ma chemical weathering history, the grain size dependence of chemical weathering intensity, and its implications for provenance change of the Chinese loess–red clay deposit. Quat. Sci. Rev. 29, 1911–1922.
Yan, Q., Zhang, Z.S., Wang, H.J., Gao, Y.Q., Zheng, W.P., 2012. Set-up and preliminary results of mid-Pliocene climate simulations with CAM3.1. Geosci. Model Dev. 5, 289–297.
Yang, S., Ding, Z., 2001. Seven million-year iron geochemistry record from a thick eolian red clay-loess sequence in Chinese Loess Plateau and the implications for paleo-monsoon evolution. Chin. Sci. Bull. 46, 337–340.
Yang, Y., Fang, X., Galy, A., Appel, E., Li, M., 2013. Quaternary paleolake nutrient evolution and climatic change in the western Qaidam Basin deduced from phosphorus geochemistry record of deep drilling core SG-1. Quat. Int. 313–314, 156–167.
Yang, S., Ding, Z., Feng, S., Jiang, W., Huang, X., Guo, L., 2018. A strengthened East Asian summer monsoon during Pliocene warmth: evidence from 'red clay' sediments at Pianguan, northern China. J. Asian Earth Sci. 155, 124–133.
Zeng, M., Song, Y., An, Z., Chang, H., Li, Y., 2014. Clay mineral records of the Erlangjian drill core sediments from the Lake Qinghai Basin, China. Sci. China Earth Sci. 57, 1846–1859.
Zhang, Z., Yan, Q., 2012. Pre-industrial and mid-Pliocene simulations with NorESM-L: AGCM simulations. Geosci. Model Dev. 5, 1033–1043.
Zhang, Y.G., Ji, J., Balsam, W., Liu, L., Chen, J., 2009. Mid-Pliocene Asian monsoon intensification and the onset of Northern Hemisphere glaciation. Geology 37, 599–602.
Zhang, Z.S., Nisancioglu, K., Bentsen, M., Tjiputra, J., Bethke, I., Yan, Q., Risebrobakken, B., Andersson, C., Jansen, E., 2012. Pre-industrial and mid-Pliocene simulations with NorESM-L. Geosci. Model Dev. 5, 523–533.
Zhang, R., Yan, Q., Zhang, Z.S., Jiang, D., Otto-Bliesner, B.L., Haywood, A.M., Hill, D.J., Dolan, A.M., Stepanek, C., Lohmann, G., Contoux, C., Bragg, F., Chan, W.L., Chandler, M.A., Jost, A., Kamae, Y., Abe-Ouchi, A., Ramstein, G., Rosenbloom, N.A., Sohl, L., Ueda, H., 2013. Mid-Pliocene East Asian monsoon climate simulated in the PlioMIP. Clim. Past 9, 2085–2099.
Zheng, W., Zhang, Z., Chen, L., Yu, Y., 2013. The mid-Pliocene climate simulated by FGOALS-g2. Geosci. Model Dev. 6, 1127–1135.
Zheng, Y., Zhang, J., Wang, J., Zhang, B., Wang, X., Wang, M., 2014. Rapid denudation of the Himalayan orogen in the Nyalam area, southern Tibet, since the Pliocene and implications for tectonics–climate coupling. Chin. Sci. Bull. 59, 874–885.